Christina Stumpf

Importance-Truncated Large-Scale Shell Model

Master Thesis

Supervisor Prof. Dr. Robert Roth
Second Advisor MSc. Angelo Calci

February 2013

TECHNISCHE
UNIVERSITÄT
DARMSTADT

Contents

Chapter 1

Introduction

Nuclear structure theory aims at a detailed understanding of the atomic nucleus at the quantum level. One approach is to choose a deliberately simplified theory that is mathematically tractable but rich in physical insight. If this theory accounts for at least some nuclear properties, it can be improved by adding new terms. In this way, models have been developed which try to approximate the interactions inside atomic nuclei and, if close to reality, describe nuclear properties precisely. This implies an accurate reproduction of experimental observables, e.g. binding and excitation energies, as well as quantitative predictions where no experimental data is available. Experiments have provided information on nuclei mainly near the island of stability. In the past years, exotic nuclei have become of particular interest in nuclear astrophysics as they play a crucial role in the processes of stellar nucleosynthesis.

Theoretical models have often been inspired by experiments and shall, in return, provide a guideline for future experiments. One prominent example is the naive shell model: Since there are, in general, no analytical solutions for a system of A interacting particles, the system is approximately described in terms of A independent particles moving in a central field. This central field accounts for the average action of all particles on one given particle, while the mutual interaction between the particles has to be considered explicitely via a residual interaction. The name "naive shell model", or also termed "independent-particle model", is due to the fact that independent fermions in the central field exhibit some shell structure. Shells consist of one or several single-particle orbits defined by their single-particle energy. They are characterized by the energy gaps between two shells which are larger than the energy differences between the orbits within a shell. If one considers a closed-shell state, i.e. all orbits of a certain shell are fully occupied, excitations are only possible by exciting one particle to another shell. Therefore, closed-shell states are especially stable.

At first glance, it is not evident that the shell model can be applied to the atomic

nucleus as has been done for the electron system of the atom. Nuclei are self-bound systems consisting of A interacting nucleons without a defined reference point. The puzzle can be resolved in the following way: We can add a Hamiltonian acting exclusively on the center of mass of the nucleus to the nuclear Hamiltonian without changing its intrinsic properties. If we choose this center-of-mass Hamiltonian to be a harmonic-oscillator potential, we obtain a harmonic central field as natural starting point. In this way, the atomic nucleus is confined to a limited portion of space. In fact, we could also use a potential that is not a pure harmonic-oscillator potential but a modification of it, so that e.g. the separation energy for a nucleon is not infinite.

The applicability of the shell model to the atomic nucleus is valid and has been confirmed experimentally. The observation of high-lying first excited states for some even-even nuclei in comparison to neighboring even-even nuclei indicates relatively large energy gaps between single-particle orbits for particular proton and neutron numbers, the so-called "magic numbers". In the 1950's, it became clear that spin-orbit splitting has to be taken into account to reproduce higher magic numbers [1, 2].

The aforementioned observations and ideas form the basis of the more elaborate no-core shell model (NCSM) and (valence-space) shell model. The results obtained in shell-model calculations show remarkable agreement with the experimental data. In the following, we are going to focus on the (valence-space) shell model. It is assumed that closed-shell nuclei are inert and that the nucleons inside the closed shell, composing the so-called core, do not primarily contribute to the nuclear properties. The only degrees of freedom are the valence nucleons, the nucleons outside the core, restricted to one or several (sub-)shells. The standard procedure for the description of an atomic nucleus in the framework of the shell model is to define a suitable model space, spanned by Slater determinants constructed from the single-particle states of the valence nucleons, and an interaction adapted to it. This nuclear interaction has to be transformed into an effective one to account e.g. for the influence of the core on the valence nucleons. Eigenstates of the system are obtained by diagonalizing the Hamilton matrix, which is equivalent to the solution of the Schrödinger equation. This is a computationally demanding and non-trivial task because the model-space sizes, i.e. the dimension of the Hamilton matrices, are in general very large and grow rapidly with increasing valence-particle number and the inclusion of more valence orbitals. As we are only interested in the few lowest eigenvalues, Lanczos algorithms are an efficient tool for matrix diagonalizations, and model-space dimensions of up to 10^{10} [3] become tractable, e.g. using the Antoine code [4].

Shell-model calculations within a full model space, i.e. a model space with no further restrictions than the allowed valence orbits, are often not feasible and have to be

carried out in a truncated model space, where convergence is not guaranteed. Furthermore, if we are only interested in a few eigenstates, many of the basis states turn out to be negligible for the description of the target states. If we discarded these basis states from the outset, we would reduce the model-space size significantly while leaving the quality of the results almost unchanged and extending the shell model to larger model spaces. This approach was first developed in quantum chemistry in the 1970's and has successfully been applied to nuclear structure theory in the framework of the no-core shell model [5]. An importance measure derived from multi-configurational perturbation theory is employed to estimate the relevance of each basis state for the basis expansion of a target state. Basis states with an importance measure smaller than a given importance threshold are considered dispensable and are not included in the model space. In [5], the 0^+ ground-state energies of various closed- and open-shell nuclei in the p shell have been computed via the importance-truncated no-core shell model (IT-NCSM). Full NCSM calculations can be performed routinely for ^{16}O using model spaces which include many-body states with unperturbed excitation energies of up to $N_{\max}\hbar\omega = 8\hbar\omega$, corresponding to a dimension of approximately $0.6 \cdot 10^9$. Model spaces with larger $N_{\max}$ are beyond the reach of present NCSM codes. The importance truncation allows for a treatment of model spaces of $N_{\max} = 22$ and beyond. In this case, the actual limit is not imposed by the basis dimension itself but is due to the matrix elements available for the interaction used in this calculation. Absolute energies obtained in IT-NCSM calculations deviate only by a few 100 keV from the exact NCSM results where the NCSM is still feasible, while reducing the model space size dramatically, e.g. for $N_{\max} = 8$, dimensions are reduced by two orders of magnitude. Note that excitation energies are reproduced even more accurately. The full model space and the exact NCSM results can be recovered in the limit of vanishing importance threshold. Therefore, the diagonalization in the IT model space gives a variational approximation to the eigenstate obtained in the full model space. In analogy to the NCSM, we apply the importance-truncation scheme to the shell model and extend it to larger valence spaces.

This thesis is organized as follows: In Chapter 2, we give an introduction to the valence-space shell model. Ideally, an eigenstate of a nucleus factorizes into a center-of-mass and intrinsic component. This is not the case in the shell model and can give rise to center-of-mass contaminations. We explain this problem and present an approximate solution in Chapter 3. In Chapter 4, we explain the importance-truncation scheme and apply it to the (valence-space) shell model. As first test cases, we consider the nuclei ^{56}Ni and ^{64}Ge in the pf shell and $pfg_{9/2}$ shell, respectively. We present the results in Chapter 6. For ^{56}Ni, we compare the energies and observables computed

in the framework of the importance-truncated shell model to the exact values. Since ^{64}Ge is already beyond the reach of standard shell-model calculations, we compare the results to values obtained in the Monte-Carlo shell model [6], where a stochastic approach is made to solve the nuclear many-body problem. An introduction to this topic is given in Chapter 5.

Chapter 2

Valence-Space Shell Model

The shell model is a successful tool for the spectroscopic description of atomic nuclei. Light nuclei with mass number $A \lesssim 13$ can be treated exactly in the framework of the no-core shell model [5] whereas medium-mass and heavy nuclei can be described approximately in the (valence-space) shell model.

A brief summary of the development of the shell model is given in Chapter 1. In the following, we discuss the basic assumptions and the general procedure of a valence-space shell-model calculation.

First, one needs to define and construct the model space, also termed valence space (see Section 2.1). Since this model space is a subspace of the full Hilbert space, an effective interaction is derived from a realistic nucleon-nucleon potential, which accounts for effects of configurations excluded from the model space, see Section 2.2. In the last step, the eigenvalue problem of the effective Hamiltonian is solved in the valence space. As we are only interested in a few low-lying eigenstates, the Lanczos algorithm (see Section 2.3) is an efficient tool for the diagonalization of the Hamilton matrix. In Section 2.4, we give some remarks on present shell-model calculations and their challenges.

2.1. The Model Space

In the naive shell model, the nucleus is approximated by a system of A nucleons confined in a central potential in combination with a spin-orbit term [1, 2].

For convenience, we adopt the harmonic-oscillator single-particle potential as central potential, but other choices, such as the Woods-Saxon potential, are possible [7]. The eigenstates of the central potential are the single-particle orbits $0s_{1/2}$, $0p_{3/2}$, $0p_{1/2}$, ... (see Figure 2.1). Note that these single-partice eigenstates also carry the z-projections of

the total angular momentum, m, and the isospin, m_t, as quantum numbers.

These single-particle orbits are grouped in so-called shells according to their single-particle energy in such a way that energy differences between orbits within one shell are much smaller than energy differences between orbits of two different shells. The spin-orbit term causes a lowering in energy of orbits with large coupled momentum $j = l + s$, see e.g. $0f_{7/2}$ and $0g_{9/2}$ in Figure 2.1, and gives rise to shell closures that reproduce the experimentally observed magic numbers 2, 8, 20, 28, 50, 82 and 126.

Nuclei with magic neutron and proton numbers are especially stable: In absence of the mutual interaction, all the nucleons occupy the lowest single-particle orbits allowed according to the Pauli principle up to a shell gap at a magic number, and excitations are only possible if one or more nucleons are excited to a higher shell.

When describing an atomic nucleus in the valence-space shell model, we first classify its nucleons as core and valence nucleons. The nucleons inside the fully occupied closed shells compose the so-called core ($J^\pi = 0^+$), which can be different for neutrons and protons. The core nucleons are inert: They have no primary contribution to the nuclear properties. They are thus not considered explicitly, but some of their effects are included approximately in the effective interaction between the valence nucleons (see Section 2.2).

The only degrees of freedom are the valence nucleons, which are restricted to one or a few (sub-)shells above the core. Single-particle orbits with higher single-particle energy than the valence orbits are not neglected but their effects are accounted for implicitly via a renormalization process of the effective interaction.

In Figure 2.1, we illustrate the core and valence orbits. Here, we assume the single-particle orbits of the neutrons and protons to be fully occupied up to the shell closure at the magic number 20. These nucleons compose a ^{40}Ca core. We take the single-particle orbits $0f_{7/2}$, $1p_{3/2}$, $0f_{5/2}$, $1p_{1/2}$ and $0g_{9/2}$ as valence orbits. These orbits are partly occupied by the valence nucleons, which are treated as explicit degrees of freedom. If we consider a ^{56}Ni nucleus, we assume 20 protons and 20 neutrons to form a ^{40}Ca core and 8 neutrons and 8 protons that occupy the aforementioned valence orbits.

The model space is spanned by Slater determinants $|\Phi_\nu\rangle$ built from the single-particle states of the valence nucleons. A nuclear many-body basis state can be written as

$$|\Phi_{\mathrm{nuc},\nu}\rangle = |\Phi_{\mathrm{core}}\rangle \otimes |\Phi_\nu\rangle \,, \tag{2.1}$$

where the core state $|\Phi_{\mathrm{core}}\rangle$ is a single Slater determinant and is identical for all configurations, i.e. basis states. As it is not taken into account explicitly in shell-model calculations, we only consider the Slater determinants of the valence nucleons $|\Phi_\nu\rangle$ and obtain results relative to the core.

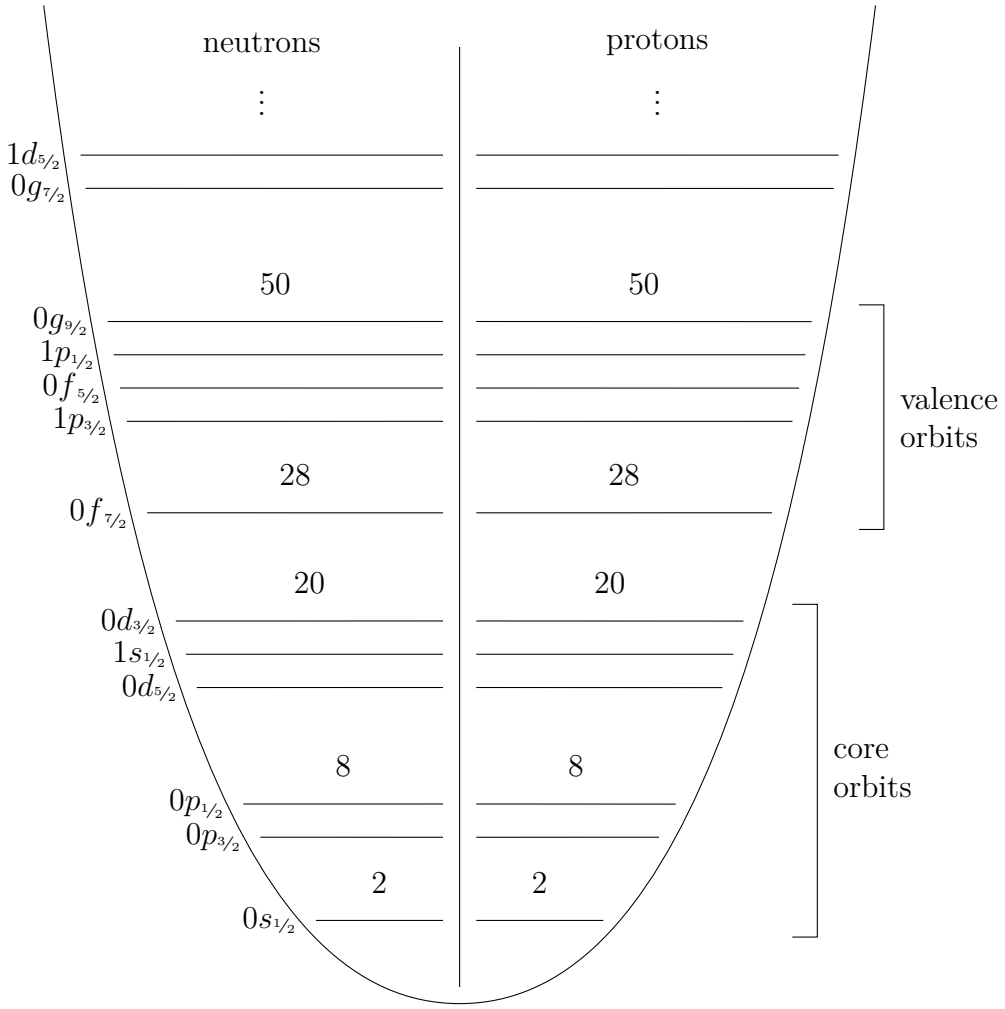

Figure 2.1.: Single-particle orbits and magic numbers for neutrons and protons in the (spherical) shell model generated by a harmonic-oscillator potential with spin-orbit term. As an example, a ^{40}Ca core and five valence orbits ($0f_{7/2}$, $1p_{3/2}$, $0f_{5/2}$, $1p_{1/2}$ and $0g_{9/2}$) are indicated.

Each basis state $|\Phi_\nu\rangle$ has a definite value of the z-projection M of the total angular momentum J,

$$M = \sum_{i=1}^{A_{\text{val}}} m_i, \tag{2.2}$$

where the sum runs over all valence nucleons. In the following, we use the m-scheme and include only configurations with a given value of M in the model space. The number of Slater determinants in such a model space is referred to as m-scheme dimension. The main advantage of using this basis is the simplicity of computing the matrix elements, which reduce to sums of two-body (2B) matrix elements for a 2B Hamiltonian. Another possible choice of basis is the JT-coupled scheme [4].

Model-space dimensions increase rapidly when going to heavier nuclei or including

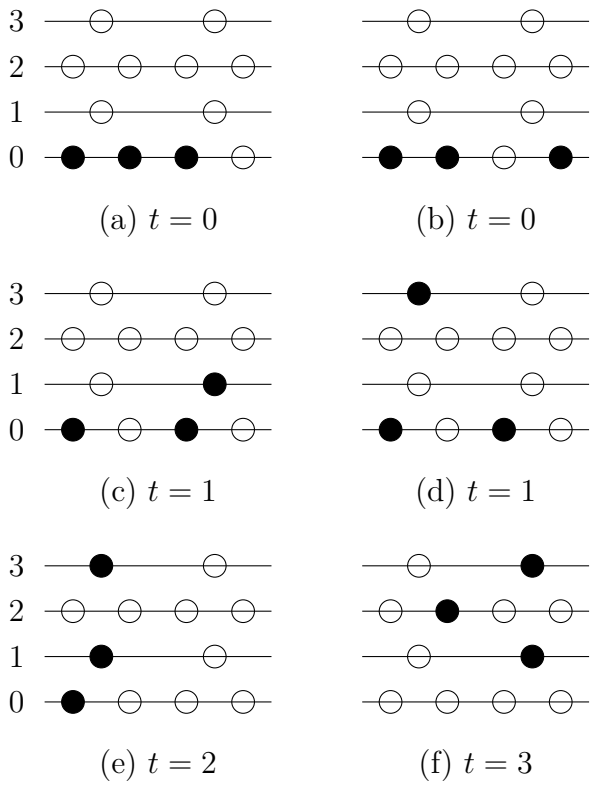

Figure 2.2.: Examples for some t configurations in a schematic valence space: (a) and (b) states with $t = 0$, (c) and (d) states with $t = 1$, (e) state with $t = 2$ and (f) state with $t = 3$. Open and filled circles denote unoccupied and occupied single-particle states, respectively.

more single-particle orbits in the valence space, and shell-model calculations become intractable. In standard shell-model calculations, the so-called $T_{\max}$-truncation is introduced to cope with this problem: Each configuration has an assigned value t which denotes the number of nucleons that are excited to energetically higher valence orbits compared to the lowest possible configurations. In the $T_{\max}$-truncated model space, we only include basis states with $t \leq T_{\max}$.

Some configurations with different values of t are illustrated schematically in Figure 2.2. Each of the six pictures shows four valence orbits for one particle species. Open and filled circles denote unoccupied and occupied single-particle states, respectively. In the lowest possible configurations ($t = 0$), the three particles occupy orbit 0. By exciting one particle from orbit 0 to an orbit with higher single-particle energy, i.e. orbit 1, 2 or 3, we obtain configurations with $t = 1$, where it is irrelevant to which of the higher valence orbits the nucleon is excited. In the same way, we can construct configurations with $t = 2$, $t = 3$ and up to $t = T_{\max}$.

We remark that the single-particle states and energies, in practice, are not related

to any central potential. Although we use spherical single-particle states as bases, the corresponding energies are typically replaced by single-particle excitation energies determined in experiments. However, we adopt the common picture of a central potential for simplicity, and implicitly identify the eigenenergies of this central potential with the single-particle energies taken from experiment [8].

2.2. The Effective Interaction

For nuclei with two or more valence nucleons on top of the core, we need to take into account the residual two-body interaction between the valence nucleons, i.e. the part of the interaction which is not already absorbed in the single-particle energies. This residual interaction lifts the degeneracy of the configurations which are constructed from single-particle states of the same valence orbits and causes a complex coupling between them.

For the solution of the eigenvalue problem, we need to set up and diagonalize the Hamilton matrix, which is not done in the full Hilbert space but in the finite valence space. We thus have to transform the residual interaction into an effective one that is adapted to this finite model space.

Starting point for its derivation is a free nucleon-nucleon (NN) potential $\mathbf{V}_{\mathrm{NN}}$, either of phenomenological origin, e.g. the Argonne V18 potential [9] and the Bonn potentials [10], or constructed in the framework of chiral effective field theory (e.g. [11, 12]). These potentials are all realistic potentials, i.e. they reproduce the NN scattering data and deuteron binding energy accurately. One common feature of these realistic interactions is the strong repulsive core, which prevents their direct use in nuclear structure calculations: The repulsive core gives rise to short-range correlations, which pose a problem when calculating the effective interaction perturbatively order-by-order [8, 13]. Therefore, we need to renormalize the realistic interactions before computing the effective interaction.

The traditional approach for the renormalization of $\mathbf{V}_{\mathrm{NN}}$ is the G-matrix formalism [14, 15], where the NN potential is replaced by the reaction matrix $\mathbf{G}$. This reaction matrix is equivalent to the Lippmann-Schwinger equation for the scattering of two nucleons in the nuclear medium:

$$\mathbf{G}(\omega) = \mathbf{V}_{\mathrm{NN}} + \mathbf{V}_{\mathrm{NN}} \frac{\mathbf{Q}_{2p}}{\omega - \mathbf{H}_0} \mathbf{G}(\omega). \tag{2.3}$$

The variable ω denotes the starting energy and the operator $\mathbf{Q}_{2p}$ projects onto two single-particle states above the closed-shell core, either one state of the valence space

in combination with a state above the valence space or both states above the valence space. Furthermore, it accounts for the Pauli principle, i.e. it does not allow the nucleons to scatter into already occupied single-particle states. In order to compute the individual matrix elements of $\mathbf{G}$, we expand them in a series where the individual terms can be represented by ladder diagrams. Matrix elements of $\mathbf{G}$ with respect to configurations of the complementary space $\mathbf{P}_{2p} = 1 - \mathbf{Q}_{2p}$ describe a scattering sequence of two nucleons starting from and finishing in a state of the $\mathbf{P}_{2p}$ space. The intermediate states belong to the $\mathbf{Q}_{2p}$ space. Thus, the respective ladder diagrams correspond to highly excited two-nucleon states, which can be summed up. In this way, the interaction, after transformation into an effective one, accounts for single-particle states above the valence orbits.

An alternative method for the renormalization of realistic interactions is the $V_{\mathrm{low}k}$ approach [16, 17]: A low-momentum potential $V_{\mathrm{low}k}$ is constructed that preserves the physics of $\mathbf{V}_{\mathrm{NN}}$ up to a certain momentum cutoff Λ by integrating out the high-momentum components of the original potential. We define a continuum model space via

$$\mathbf{P} = \int \mathrm{d}\mathbf{p}\, |\mathbf{p}\rangle \langle \mathbf{p}|\,, \quad \mathrm{p} \leq \Lambda, \tag{2.4}$$

where $\mathbf{p}$ denotes the relative two-nucleon momentum. The momentum cutoff Λ is typically chosen to be in the vicinity of 2 fm^{-1} corresponding to an energy of 350 MeV, up to which the realistic interactions fit the empirical phase shifts. The T-matrix in the $\mathbf{P}$-space can be written as

$$T_{\mathrm{low}k}(p', p, p^2) = V_{\mathrm{low}k}(p', p) + \mathcal{P} \int_0^{\Lambda} q^2 \mathrm{dq} \mathrm{V}_{\mathrm{low}k}(\mathrm{p}', \mathrm{q}) \frac{1}{\mathrm{p}^2 - \mathrm{q}^2} \mathrm{T}_{\mathrm{low}k}(\mathrm{q}, \mathrm{p}, \mathrm{p}^2), \tag{2.5}$$

where for all momenta p, p' holds $(p, p') \leq \Lambda$. The second term of the right hand side of this Equation is the principle value of the integral. Furthermore, we require that

$$T(p', p, p^2) = T_{\mathrm{low}k}(p', p, p^2), \quad (p, p') \leq \Lambda. \tag{2.6}$$

Then, Equation (2.5) defines a low-momentum interaction. As its solution, one obtains a smooth potential suitable for nuclear structure calculations.

In a second step, the renormalized potential $\mathbf{V}_{\mathrm{NN}}^{\mathrm{ren}}$ is transformed into an effective interaction $\mathbf{V}_{\mathrm{eff}}$, i.e. an interaction defined for a particular model space which accounts for effects of excluded configurations. Ideally, the eigenvalues of the shell-model Hamiltonian in a model space are a subset of the eigenvalues of the full nuclear Hamiltonian in the entire Hilbert space. We start from the eigenvalue problem of the renormalized

realistic Hamiltonian $\mathbf{H}^{\text{ren}}$ in the full Hilbert space:

$$\mathbf{H}^{\text{ren}} |\Psi_\alpha\rangle = E_\alpha |\Psi_\alpha\rangle , \tag{2.7}$$

where

$$\mathbf{H}^{\text{ren}} = \mathbf{H}_0 + \mathbf{H}_1 \tag{2.8}$$

with

$$\mathbf{H}_0 = \mathbf{T} + \mathbf{U}, \tag{2.9}$$
$$\mathbf{H}_1 = \mathbf{V}_{\text{NN}}^{\text{ren}} - \mathbf{U}. \tag{2.10}$$

The auxiliary one-body potential $\mathbf{U}$ has been introduced in order to break up $\mathbf{H}^{\text{ren}}$ into the sum of an unperturbed Hamiltonian $\mathbf{H}_0$ chosen to make the perturbation $\mathbf{H}_1$ small. It is the central field approximating the average action of all nucleons on one given nucleon. Its eigenstates are the single-particle states of the valence nucleons. The operator $\mathbf{T}$ denotes the kinetic energy of the nucleons.

The aim of the effective-interaction theory is to reduce the eigenvalue problem (2.7) to a model-space eigenvalue problem

$$\mathbf{P}\mathbf{H}_{\text{eff}}\mathbf{P} |\Psi_n\rangle = E_n |\Psi_n\rangle , \tag{2.11}$$

where the operator

$$\mathbf{P} = \sum_{i=1}^{D} |\Phi_i\rangle \langle\Phi_i| \tag{2.12}$$

projects the complete Hilbert space onto the valence space. The model-space projector $\mathbf{P}$ and its complement $\mathbf{Q} = \mathbf{1} - \mathbf{P}$ fulfill the following relations:

$$\mathbf{P}^2 = \mathbf{P}, \quad \mathbf{Q}^2 = \mathbf{Q}, \quad \mathbf{P}\mathbf{Q} = \mathbf{Q}\mathbf{P} = 0. \tag{2.13}$$

The eigenvalues E_n and eigenstates $|\Psi_n\rangle$ are a subset of the eigenvalues and eigenstates of the full Hamiltonian, respectively.

In the following, we derive the simple Bloch-Horowitz form [18] of the effective interaction: We project the eigenvalue problem of the entire Hilbert space (2.7) onto the

model space and the excluded space:

$$\mathbf{PH}^{\text{ren}}\mathbf{P}^2\left|\Psi_\alpha\right\rangle + \mathbf{PH}^{\text{ren}}\mathbf{Q}^2\left|\Psi_\alpha\right\rangle = E_\alpha\mathbf{P}\left|\Psi_\alpha\right\rangle, \tag{2.14}$$

$$\mathbf{QH}^{\text{ren}}\mathbf{P}^2\left|\Psi_\alpha\right\rangle + \mathbf{QH}^{\text{ren}}\mathbf{Q}^2\left|\Psi_\alpha\right\rangle = E_\alpha\mathbf{Q}\left|\Psi_\alpha\right\rangle. \tag{2.15}$$

From Equation (2.15), we obtain an expression for

$$\mathbf{Q}\left|\Psi_\alpha\right\rangle = \frac{1}{E_\alpha - \mathbf{QH}^{\text{ren}}\mathbf{Q}}\mathbf{QH}^{\text{ren}}\mathbf{P}^2\left|\Psi_\alpha\right\rangle, \tag{2.16}$$

which can be inserted into (2.14):

$$\left(\mathbf{PH}^{\text{ren}}\mathbf{P} + \mathbf{PH}^{\text{ren}}\mathbf{Q}\frac{1}{E_\alpha - \mathbf{QH}^{\text{ren}}\mathbf{Q}}\mathbf{QH}^{\text{ren}}\mathbf{P}\right)\mathbf{P}\left|\Psi_\alpha\right\rangle = E_\alpha\mathbf{P}\left|\Psi_\alpha\right\rangle. \tag{2.17}$$

By comparing this relation with (2.11), we can identify the effective Hamiltonian

$$\mathbf{H}_{\text{eff}}(E_\alpha) = \mathbf{PH}^{\text{ren}}\mathbf{P} + \mathbf{PH}^{\text{ren}}\mathbf{Q}\frac{1}{E_\alpha - \mathbf{QH}^{\text{ren}}\mathbf{Q}}\mathbf{QH}^{\text{ren}}\mathbf{P}. \tag{2.18}$$

Since the projection operators $\mathbf{P}$ and $\mathbf{Q}$ commute with the unperturbed Hamiltonian $\mathbf{H}_0$, we can find an expression for the effective interaction $\mathbf{V}_{\text{eff}}$:

$$\mathbf{H}_{\text{eff}}(E_\alpha) = \mathbf{PH}_0\mathbf{P} + \mathbf{V}_{\text{eff}}(E_\alpha), \tag{2.19}$$

$$\mathbf{V}_{\text{eff}}(E_\alpha) = \mathbf{PH}_1\mathbf{P} + \mathbf{PH}_1\mathbf{Q}\frac{1}{E_\alpha - \mathbf{QH}^{\text{ren}}\mathbf{Q}}\mathbf{QH}_1\mathbf{P}. \tag{2.20}$$

Expansion of the denominator yields the Bloch-Horowitz form of the effective interaction:

$$\mathbf{V}_{\text{eff}}(E_\alpha) = \mathbf{PH}_1\mathbf{P} + \mathbf{PH}_1\frac{\mathbf{Q}}{E_\alpha - \mathbf{QH}_0\mathbf{Q}}\mathbf{V}_{\text{eff}}(E_\alpha). \tag{2.21}$$

This definition of the effective interaction is simple, but its practical application is not because the interaction depends on the eigenvalue and one would need to derive different effective Hamiltonians for different eigenvalues.

This energy dependence can be eliminated in the $\hat{Q}$-box formalism: The energy denominator is expanded and the terms of its series are rearranged. Then, the so-called folded diagrams [19] are introduced, which remove the energy dependence. The folded-diagram series is then partially summed up using an iterative method, e.g. the Lee-Suzuki transformation [20].

We remark that we do not use the eigenenergies of the unperturbed Hamiltonian as effective single-particle energies. Since the eigenvalues of $\mathbf{H}_0$ represent the energies of

a nucleus with one valence nucleon relative to the core, we identify the single-particle energies of the effective Hamiltonian with experimental excitation energies.

Detailed reviews on the derivation of realistic effective interactions are given in [21, 8, 22].

2.3. The Solution of the Schrödinger Equation – The Lanczos Algorithm

In order to obtain the eigenvalues and eigenstates of the Hamiltonian, we need to compute and diagonalize the Hamilton matrix, which is equivalent to the solution of the Schrödinger equation

$$\mathbf{H}\,|\Psi_n\rangle = E_n\,|\Psi_n\rangle \tag{2.22}$$

in a finite model space. The Hamiltonian $\mathbf{H}$ is given by the effective interaction derived above.

Standard diagonalization methods are not well-suited for the diagonalization of Hamilton matrices in large-scale shell-model calculations because all matrix elements need to be stored. Furthermore, the CPU time scales cubically with the dimension of the model space. In shell-model calculations, the Hamilton matrices are typically very sparse and one is usually only interested in one or a few low-lying eigenstates. In these cases, the Lanczos algorithm [23, 24, 25] – an efficient tool for the solution of large sparse eigenvalue problems – can be used and model-space dimensions of up to 10^{10} become tractable in common shell-model codes.

The Lanczos algorithm, i.e. the Arnoldi algorithm for hermitian matrices, is an orthogonal projection method onto Krylov spaces designed to find approximations for a few specified eigenvalues and eigenstates in these subspaces. This algorithm constructs an orthogonal basis in which the Hamilton matrix is tridiagonal, i.e., it has only non-vanishing matrix elements on the main diagonal and on the first diagonal below and above the main diagonal:

$$H = \begin{pmatrix} H_{1,1} & H_{1,2} & 0 & \cdots & 0 \\ H_{2,1} & H_{2,2} & H_{2,3} & & \\ 0 & H_{3,2} & H_{3,3} & H_{3,4} & \vdots \\ & & & & \\ \vdots & & \ddots & \ddots & \ddots \\ & & & & H_{m-1,m} \\ 0 & \cdots & 0 & H_{m,m-1} & H_{m,m} \end{pmatrix}. \tag{2.23}$$

The index m denotes the dimension of the orthogonal basis, which is constructed iteratively: Starting point is the so-called "pivot state" $|v_1\rangle$, e.g. a random linear combination of basis Slater determinants. The Hamilton operator is applied to the pivot state and the resulting vector is decomposed into its projection onto the pivot state and a normalized vector $|v_2\rangle$ orthogonal to it:

$$\mathbf{H}\,|v_1\rangle = H_{1,1}\,|v_1\rangle + H_{1,2}\,|v_2\rangle\,. \tag{2.24}$$

The coefficients $H_{1,1}$ and $H_{1,2}$ are matrix elements of (2.23):

$$H_{1,1} = \langle v_1|\mathbf{H}|v_1\rangle \tag{2.25}$$

$$H_{1,2} = \langle v_1|\mathbf{H}|v_2\rangle\,. \tag{2.26}$$

In the same way, the basis state $|v_{k+1}\rangle$ can be constructed using the previously constructed basis states $|v_{k-1}\rangle$ and $|v_k\rangle$,

$$\mathbf{H}\,|v_k\rangle = H_{k,k-1}\,|v_{k-1}\rangle + H_{k,k}\,|v_k\rangle + H_{k,k+1}\,|v_{k+1}\rangle\,, \tag{2.27}$$

where

$$H_{k,k} = \langle v_k|\mathbf{H}|v_k\rangle\,, \tag{2.28}$$

$$H_{k,k+1} = \langle v_k|\mathbf{H}|v_{k+1}\rangle = \langle v_{k+1}|\mathbf{H}|v_k\rangle\,, \tag{2.29}$$

$$H_{i,j} = 0 \quad \text{for } |i-j| > 1. \tag{2.30}$$

The relations (2.29) and (2.30) hold because the Hamiltonian $\mathbf{H}$ is hermitian and so must be the iteratively constructed Hamilton matrix H in any step of the iteration. One obtains the real symmetric matrix H (2.23), which is diagonalized in each iteration. Since this matrix is tridiagonal, the computation of the eigenvalues and eigenstates can be carried out efficiently by standard diagonalization methods, e.g. the QR algorithm. In principle, a new Lanczos vector $|v_{k+1}\rangle$ only needs to be reorthogonalized with respect to the two preceeding ones because it is already orthogonal to all other basis states by construction. However, this does not hold true in practice due to numerical errors and the basis state $|v_{k+1}\rangle$ has to be reorthogonalized to all previously computed basis states in each iteration. This process is continued until all the required eigenvalues are converged, i.e. the inclusion of additional basis states does not affect the eigenvalues anymore. In the course of the iteration, low-lying extremal energy eigenvalues converge first.

For large-scale eigenvalue problems, the original and simple Lanczos algorithm de-

scribed above runs into intractable storage and computational requirements. Therefore, our shell-model code uses the more sophisticated implementation of the Lanczos algorithm provided by the ARPACK library, the implicitly restarted Arnoldi method [26]. The basic idea of this implicit restarting scheme is, once the standard Lanczos algorithm has constructed an m dimensional Krylov space, to compress the important information into a $k < m$ dimensional subspace of the Krylov space. This is accomplished by a repeated application of the implicitly shifted QR algorithm to the $m \times m$ dimensional Hamilton matrix. Only the first k basis states are kept, of which the last one is employed as updated starting vector for the Lanczos algorithm used to recompute the missing $m - k$ basis vectors. This procedure ist carried out until all required eigenvalues are converged. In our calculations, typically ten to 15 restarts are necessary to obtain the ground-state energy.

2.4. Some Remarks on Shell-Model Calculations

The valence-space shell model has been applied successfully to medium-mass and heavy nuclei. A detailed review of the model and its applications is given in [21]. Nowadays, model-spaces containing up to 10^{10} basis states can be treated. This limit is due to the Lanczos algorithm, which requires sufficient storage for the components of the Lanczos vectors.

We can estimate the m-scheme shell-model dimension D via

$$D = \binom{N_n}{n_n} \cdot \binom{N_p}{n_p} \cdot f, \tag{2.31}$$

where n_n and n_p denote the number of valence neutrons and protons that can occupy N_n and N_p neutron and proton single-particle states of the valence orbits, respectively. The factor f accounts for the fraction of Slater determinants that have proper values of M and given parity, and that are included in the model space. Equation (2.31) illustrates that the model-space size increases rapidly when including more valence nucleons and single-particle orbits in the valence space.

To overcome the problem of intractably large model spaces, shell-model calculations are often carried out in T_{max}-truncated model spaces. But since the effective interaction is always adapted to one particular full model space (Section 2.2), results obtained in calculations using truncated and full model spaces can be quite different if the former are not converged with respect to T_{max}. Furthermore, convergence with respect to T_{max} is slow, especially for excited states.

Figure 2.3 illustrates the aforementioned: The energies of the first 0^+, 2^+, 4^+ and

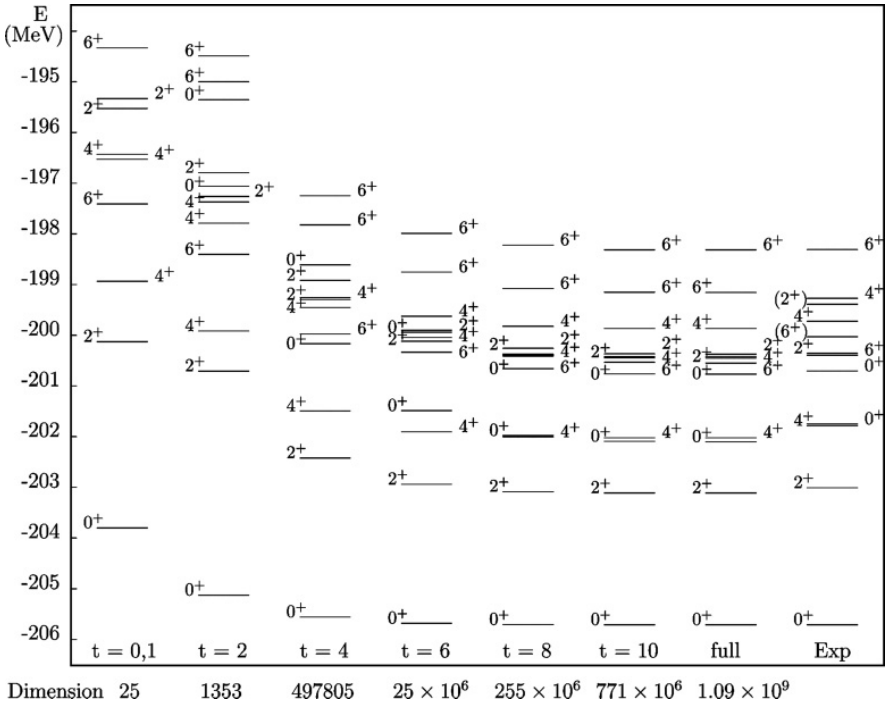

Figure 2.3.: Evolution of the first three 0^+, 2^+, 4^+ and 6^+ states of ^{56}Ni as a function of $t = T_{\max}$ in the $T_{\max}$-truncated and full pf model space using the GXPF1A interaction [27]. In the last column, experimental excitation energies are shown. Figure taken from [28].

6^+ states of ^{56}Ni are shown as a funcion of $T_{\max}$. The shell-model energies computed in the full model space are in excellent agreement with the experimental spectrum. But the dimension of the full model space is 1.09×10^9 and is at the limit of a feasible shell-model calculation. The energies obtained in shell-model calculations that are carried out in truncated model spaces can show quite different patterns if compared to those of the full model space: For $T_{\max} = 2$ and $T_{\max} = 4$, they are still far from convergence, e.g. the first excited 0^+ and the lowest 4^+ state have a quite large energy difference whereas they are rather close together in the case of the full model space. The energies are not converged until $T_{\max} = 10$, where the model space already contains 771×10^6 basis states.

By restricting shell-model calculations to $0\hbar\omega$ model spaces, e.g. the pf shell, we can only describe a limited number of low-lying states of the same parity. To access all observables of interest, such as E1 transitions that imply states of different parity, we need to handle valence spaces including single-particle states from different contiguous major shells, e.g. the pf shell and the $0g_{9/2}$ orbit. Such model spaces often become intractably large depending on the nucleus to describe and suffer from center-of-mass contaminations.

There are renowned shell-model codes, e.g. the m-scheme codes ANTOINE [21] and MSHELL [29], that fully exploit the computational resources. Nowadays, the development of shell-model calculations depends mainly on advances in computer technology. The shell-model codes have been keeping up with these advances: Computations have become faster by a factor of 10^5 between 1970 and 2000. In the same period of time, the dimension that can be handled in shell-model calculations has become 10^5 times larger [6].

Although the computer technology and the quality of shell-model codes is improved, many nuclei will remain out of reach of conventional shell-model calculations in the future.

Chapter 3

Center-of-Mass Problem

The quantum-mechanical description of an atomic nucleus poses a challenge because one has to deal with a finite self-bound system without defined reference point. In the exact theory, the problem is as follows: The nucleus' state $|\Psi\rangle$ depends on the coordinates and momenta of the A nucleons. For the description of the intrinsic properties of a nucleus, one needs the relative positions and momenta of the nucleons, i.e. $3A-3$ coordinates and $3A-3$ momenta. The redundant coordinates and momenta account for the motion of the center of mass. Any intrinsic operator $\mathbf{O}_{\text{int}}$ is translationally invariant and commutes with the center-of-mass momentum operator: $[\mathbf{O}_{\text{int}}, \mathbf{P}] = 0$. Furthermore, Galilean invariance applies and the operator also commutes with the center-of-mass coordinate: $[\mathbf{O}_{\text{int}}, \mathbf{R}] = 0$. Thus, any physical operator $\mathbf{O}_{\text{int}}$, the intrinsic nuclear Hamiltonian $\mathbf{H}_{\text{nuc}}$ in particular, and an operator acting on the center of mass of the nucleus possess a common eigenbasis and the many-body eigenstate factorizes:

$$|\Psi\rangle = |\Psi_{\text{cm}}\rangle \otimes |\Psi_{\text{int}}\rangle \,. \tag{3.1}$$

The states $|\Psi_{\text{int}}\rangle$ and $|\Psi_{\text{cm}}\rangle$ depend only on relative and center-of-mass coordinates and momenta, respectively. When solving the eigenvalue problem for the nuclear Hamiltonian $\mathbf{H}_{\text{nuc}}$, eigenstates with the same intrinsic component $|\Psi_{\text{int}}\rangle$ but different center-of-mass component $|\Psi_{\text{cm}}\rangle$ are degenerate.

In the shell model, the basis is subject to restrictions and the eigenstates do not factorize. Furthermore, the nuclear Hamiltonian is not translationally invariant because the central potential confines the system to one point in space. Thus, the action of the nuclear Hamiltonian on an eigenstate of the nucleus also affects the center-of-mass component, which, in return, can cause a change in the energies.

In the following, we explain a solution for the center-of-mass problem in the exact theory. We apply the same procedure to the shell model in order to approximately

resolve the center-of-mass problem , see Section 3.1.

This method implies the definition of a Hamiltonian $\mathbf{H}_{\text{cm}}$ that acts exclusively on the nucleus' center of mass. In Section 3.2, we derive an expression for this Hamiltonian so that it can be handled in the shell model, where we distinguish between core and valence nucleons.

3.1. Remedy for the Center-of-Mass Problem

In order to handle the problem of spurious states, we use a Hamiltonian $\mathbf{H}$ composed of the intrinsic Hamiltonian $\mathbf{H}_{\text{nuc}}$ and a Hamiltonian $\mathbf{H}_{\text{cm}}$ acting exclusively on the nucleus' center of mass for the solution of the nuclear eigenvalue problem [30]:

$$\mathbf{H} = \mathbf{H}_{\text{nuc}} + \beta \mathbf{H}_{\text{cm}}. \tag{3.2}$$

If the model space allows for a decoupling of the intrinsic and center-of-mass components, this choice of Hamiltonian leaves the intrinsic properties of the eigenstates unchanged but confines the center-of-mass components to be in a specific state. The strength of $\mathbf{H}_{\text{cm}}$ can be controlled by the parameter β. It is convenient to take the potential $\mathbf{H}_{\text{cm}}$ to be a harmonic-oscillator potential,

$$\mathbf{H}_{\text{cm}} = \frac{\mathbf{P}^2}{2Am} + \frac{m\omega^2 A}{2}\mathbf{R}^2 - \frac{3}{2}\hbar\omega, \tag{3.3}$$

where the last term defines the ground-state energy of $\mathbf{H}_{\text{cm}}$ to be zero. By solving the eigenvalue problem using the Hamiltonian (3.2), the degeneracy of the intrinsic states with respect to their center-of-mass component is lifted. We identify eigenstates which have their center-of-mass component in the ground state as physical states and call those states which have the same intrinsic component but an excited center-of-mass component spurious states. For $\beta > 0$, these spurious states are pushed upwards in energy and are removed from the computed spectrum. If we use a $0\hbar\omega$ model space, i.e. all nucleons occupy the lowest possible harmonic-oscillator levels, the nucleus' center of mass is guaranteed to be in its ground state and the center-of-mass motion can be ignored. The center-of-mass motion must be taken into account when using a model space where the nucleons do not only occupy the lowest possible oscillator levels. When using a ^{40}Ca core and the pf shell as valence space, e.g., there are no center-of-mass contaminations possible because all nucleons occupy the lowest possible oscillator orbits ($0\hbar\omega$ space). In contrast, if we use a ^{16}O core and the $sdpf$ shell as valence space, we would allow some, but not all of the nucleons, to be excited by $1\hbar\omega$. In this case, the center of mass can be excited and its motion has to be taken into account.

In the NCSM, the diagonalization of a translationally invariant Hamiltonian ensures the factorization of the eigenstates as in (3.1) if we include all basis states of up to a maximum number $N_{\max}$ of oscillator quanta in the model space because the eigenstates of $\mathbf{H}_{\mathrm{cm}}$ can be expanded in this basis. In this case, spurious components can be effectively removed from the model space by diagonalizing the Hamiltonian as defined in (3.2) using finite values for β.

In the (valence-space) shell model, the basis is subject to resctrictions and the eigenstates do not factorize as in (3.1). There is no exact solution for the decoupling of relative and center-of-mass components. However, we apply the method described above as an approximation: The center-of-mass Hamiltonian in the representation of a truncated basis is not the original center-of-mass Hamiltonian, but it is still related to it. There are two equally successfull approaches to assess and control the damage caused when using the variational ansatz (3.2): We can vary and choose the parameter β in such a way that the expectation value of $\mathbf{H}_{\mathrm{nuc}}$ with respect to the eigenstates of $\mathbf{H}$ is minimized [31]. Another possibility, which seems to be compatible with this ansatz, is to use fairly small values for β, e.g. $\beta = 1$ [32]. In this way, the spurious components of the model space are pushed up a bit in energy while the nonspurious ones are left relatively unchanged. We assume that most of the mixing of relative and center-of-mass components can be removed in this way.

3.2. Derivation of $\mathbf{H}_{\mathrm{cm}}$

The solution of the eigenvalue problem of the Hamiltonian $\mathbf{H}$ given in (3.2) requires the computation and diagonalization of the Hamilton matrix. In particular, we need to evaluate the matrix elements of the center-of-mass Hamiltonian

$$\mathbf{H}_{\mathrm{cm}} = \frac{\mathbf{P}^2}{2Am} + \frac{m\omega^2 A}{2}\mathbf{R}^2 - \frac{3}{2}\hbar\omega. \tag{3.4}$$

The nucleon mass and oscillator frequency are denoted by m and ω, respectively. Equation (3.4) represents an A-body operator, where the center-of-mass momentum and position operator are given by

$$\mathbf{P} = \sum_{i=1}^{A} \mathbf{p}_i, \tag{3.5}$$

$$\mathbf{R} = \frac{1}{A}\sum_{i=1}^{A} \mathbf{r}_i. \tag{3.6}$$

In the shell model, the core nucleons are not treated as explicit degrees of freedom. Therefore, we need to rewrite the center-of-mass Hamiltonian $\mathbf{H}_{\mathrm{cm}}$ for the computation of the matrix elements in such a way that the particle indices in (3.5) and (3.6) distinguish between core and valence nucleons. For the center-of-mass momentum and position operator, we obtain

$$\begin{aligned}\mathbf{P}^2 &= \left(\sum_{i=1}^{A} \mathbf{p}_i\right)^2 \\ &= \sum_{i=1}^{A} \mathbf{p}_i^2 + 2\sum_{i>j}^{A} \mathbf{p}_i\mathbf{p}_j \\ &= \mathbf{P}_c^2 + 2\sum_{c=1}^{N_c}\sum_{v=N_c+1}^{A} \mathbf{p}_c\mathbf{p}_v + 2\sum_{v>v'=N_c+1}^{A} \mathbf{p}_v\mathbf{p}_{v'} + \sum_{v=N_c+1}^{A} \mathbf{p}_v^2, \end{aligned} \tag{3.7}$$

$$A^2\mathbf{R}^2 = N_c^2\mathbf{R}_c^2 + 2\sum_{c=1}^{N_c}\sum_{v=N_c+1}^{A} \mathbf{r}_c\mathbf{r}_v + 2\sum_{v>v'=N_c+1}^{A} \mathbf{r}_v\mathbf{r}_{v'} + \sum_{v=N_c+1}^{A} \mathbf{r}_v^2. \tag{3.8}$$

The first terms in (3.7) and (3.8) are the center-of-mass momentum operator $\mathbf{P}_c$ and position operator $\mathbf{R}_c$ of the core. The harmonic-oscillator potential (3.4) is then given by

$$\begin{aligned}\mathbf{H}_{\mathrm{cm}} =& \frac{N_c}{A}\left(\frac{1}{2N_cm}\mathbf{P}_c^2 + \frac{1}{2}m\omega^2 N_c\mathbf{R}_c^2\right) \\ &+ \frac{1}{A}\sum_{v=N_c+1}^{A}\left(\frac{\mathbf{p}_v^2}{2m} + \frac{1}{2}m\omega^2\mathbf{r}_v^2\right) \\ &+ \frac{1}{A}\sum_{c=1}^{N_c}\sum_{v=N_c+1}^{A}\left(\frac{\mathbf{p}_c\mathbf{p}_v}{m} + m\omega^2\mathbf{r}_c\mathbf{r}_v\right) \\ &+ \frac{1}{A}\sum_{v>v'=N_c+1}^{A}\left(\frac{\mathbf{p}_v\mathbf{p}_{v'}}{m} + m\omega^2\mathbf{r}_v\mathbf{r}_{v'}\right) \\ &- \frac{3}{2}\hbar\omega. \end{aligned} \tag{3.9}$$

In order to evaluate the matrix elements of the center-of-mass Hamiltonian, we rewrite (3.9) so that the products of the single-particle momenta and coordinates are expressed in terms of relative single-particle momenta and coordinates:

$$\mathbf{p}_i \cdot \mathbf{p}_j = \frac{1}{2}\mathbf{p}_i^2 + \frac{1}{2}\mathbf{p}_j^2 - \frac{1}{2}\left(\mathbf{p}_i - \mathbf{p}_j\right)^2 \tag{3.10}$$

$$\mathbf{r}_i \cdot \mathbf{r}_j = \frac{1}{2}\mathbf{r}_i^2 + \frac{1}{2}\mathbf{r}_j^2 - \frac{1}{2}\left(\mathbf{r}_i - \mathbf{r}_j\right)^2. \tag{3.11}$$

Insertion of these relations yields for the third term in (3.9):

$$\begin{aligned}
&\sum_{c=1}^{N_c}\sum_{v=N_c+1}^{A}\left(\frac{\mathbf{p}_c\mathbf{p}_v}{m}+m\omega^2\mathbf{r}_c\mathbf{r}_v\right)\\
&\quad=\sum_{c=1}^{N_c}\sum_{v=N_c+1}^{A}\left(\frac{1}{2m}\left(\mathbf{p}_c^2+\mathbf{p}_v^2-(\mathbf{p}_c-\mathbf{p}_v)^2\right)+\frac{m\omega^2}{2}\left(\mathbf{r}_c^2+\mathbf{r}_v^2-(\mathbf{r}_c-\mathbf{r}_v)^2\right)\right)\\
&\quad=(A-N_c)\sum_{c=1}^{N_c}\left(\frac{\mathbf{p}_c^2}{2m}+\frac{m\omega^2}{2}\mathbf{r}_c^2\right)+N_c\sum_{v=N_c+1}^{A}\left(\frac{\mathbf{p}_v^2}{2m}+\frac{m\omega^2}{2}\mathbf{r}_v^2\right)\\
&\quad-\sum_{c=1}^{N_c}\sum_{v=N_c+1}^{A}\left(\frac{(\mathbf{p}_c-\mathbf{p}_v)^2}{2m}+\frac{m\omega^2}{2}(\mathbf{r}_c-\mathbf{r}_v)^2\right).
\end{aligned}\tag{3.12}$$

In an analogous way, we rewrite the fourth term in (3.9):

$$\begin{aligned}
&\sum_{v>v'=N_c+1}^{A}\left(\frac{\mathbf{p}_v\mathbf{p}_{v'}}{m}+m\omega^2\mathbf{r}_v\mathbf{r}_{v'}\right)\\
&\quad=\sum_{v>v'=N_c+1}^{A}\left(\frac{1}{2m}\left(\mathbf{p}_v^2+\mathbf{p}_{v'}^2\right)-\frac{1}{2m}(\mathbf{p}_v-\mathbf{p}_{v'})^2+\frac{m\omega^2}{2}\left(\mathbf{r}_v^2+\mathbf{r}_{v'}^2\right)-(\mathbf{r}_v-\mathbf{r}_{v'})^2\right)\\
&\quad=(A-N_c-1)\sum_{v=N_c+1}^{A}\left(\frac{1}{2m}\mathbf{p}_v^2+\frac{m\omega^2}{2}\mathbf{r}_v^2\right)\\
&\quad-\sum_{v>v'=N_c+1}^{A}\left(\frac{1}{2m}(\mathbf{p}_v-\mathbf{p}_{v'})^2+\frac{m\omega^2}{2}(\mathbf{r}_v-\mathbf{r}_{v'})^2\right).
\end{aligned}\tag{3.13}$$

Here, we have used the identity

$$\sum_{i>j=n+1}^{N}(x_i+x_j)=\frac{1}{2}\sum_{i\neq j=n+1}^{N}(x_i+x_j)=\frac{1}{2}\cdot 2\sum_{i\neq j=n+1}^{N}x_i=(N-n-1)\sum_{i=1+1}^{N}x_i.\tag{3.14}$$

A convenient representation of the center-of-mass Hamiltonian for the framework of the (valence-space) shell model is then given by

$$\begin{aligned}\mathbf{H}_{\mathrm{cm}} =& \frac{N_c}{A}\left(\frac{1}{2N_c m}\mathbf{P}_c^2 + \frac{1}{2}m\omega^2 N_c \mathbf{R}_c^2\right) \\ &+ \sum_{v=N_c+1}^{A}\left(\frac{\mathbf{p}_v^2}{2m} + \frac{m\omega^2}{2}\mathbf{r}_v^2\right) \\ &+ \frac{A-N_c}{A}\sum_{c=1}^{N_c}\left(\frac{\mathbf{p}_c^2}{2m} + \frac{m\omega^2}{2}\mathbf{r}_c^2\right) \\ &- \frac{1}{A}\sum_{c=1}^{N_c}\sum_{v=N_c+1}^{A}\left(\frac{1}{2m}\left(\mathbf{p}_c - \mathbf{p}_v\right)^2 + \frac{m\omega^2}{2}\left(\mathbf{r}_c - \mathbf{r}_v\right)^2\right) \\ &- \frac{1}{A}\sum_{v>v'=N_c+1}^{A}\left(\frac{1}{2m}\left(\mathbf{p}_v - \mathbf{p}_{v'}\right)^2 + \frac{m\omega^2}{2}\left(\mathbf{r}_v - \mathbf{r}_{v'}\right)^2\right) \\ &- \frac{3}{2}\hbar\omega. \end{aligned} \tag{3.15}$$

The first term of (3.15) is the harmonic-oscillator potential of the core. Since there is only one possible state for the core in the shell model, i.e. the core nucleons occupying all the lowest possible single-particle states allowed according to the Pauli principle, the expectation value of the first term is $\frac{N_c}{A}\frac{3}{2}\hbar\omega$. The third term is given by harmonic-oscillator potentials for the single-particle states of the core nucleons. These terms and the last term of (3.15) can be classified as zero-body terms because they involve no or only core nucleons, which are no degrees of freedom. The second and fourth term represent one-body operators, where the latter can be identified with an effective interaction of the valence nucleons with the core. Finally, the fifth term constitutes a two-body operator acting between the valence nucleons.

Chapter 4

Importance-Truncated Shell Model

The method of importance truncation was first used in quantum chemistry in the 1970s for the description of atoms and molecules. Since the concept is generic, it can be applied to all configuration-interaction approaches as has been done for the NCSM [5]. All these approaches share the same basic framework: The eigenvalue problem for a given Hamiltonian is solved in a model space which is spanned by a set of many-body states, usually Slater determinants. This implies the computation and numerical diagonalization of huge Hamilton matrices for large-scale model spaces (see Section 2.4).

We apply the importance-truncation scheme to the (valence-space) shell model in order to reduce the model space to those basis states that are relevant for the description of a few target eigenstates. In this way, we extend it to valence spaces and nuclei beyond the reach of the conventional shell model.

This chapter follows the detailed review on the importance truncation in [5]. The general concept of the importance-truncation scheme is explained in Section 4.1. Since the main ingredient is an importance measure derived from multi-configurational perturbation theory, we give a short introduction into this topic and present two possible choices for the importance measure, see Section 4.2 and 4.3, respectively. Using this importance measure, we construct the importance-truncated model space in an iterative way (Section 4.4). Since this model space does not include all possible basis states, we give an approximate estimate for the contribution of the excluded configurations to the energy, see Section 4.5. In Sections 4.6 and 4.7, we specify some characteristics of the importance-truncated shell model (IT-SM) and give some remarks on its implementation. Finally, we discuss how the results obtained in IT-SM calculations are evaluated. For this purpose, we introduce two extrapolation techniques, which approximately account for contributions of basis states not included in the importance-truncated valence space (Section 4.8).

4.1. General concept of the Importance Truncation

The ground state and excited states of a quantum many-body system are determined by solving the eigenvalue problem of the Hamiltonian $\mathbf{H}$,

$$\mathbf{H}\,|\Psi\rangle = E\,|\Psi\rangle\,, \tag{4.1}$$

in a typically large model space. Each eigenstate $|\Psi\rangle$ can be represented as a linear combination of the basis states $|\Phi_\nu\rangle$ which span the model space:

$$|\Psi\rangle = \sum_\nu C_\nu\,|\Phi_\nu\rangle\,. \tag{4.2}$$

In the shell model, the basis states $|\Phi_\nu\rangle$ are constructed from the single-particle states of the valence nucleons with or without $T_{\max}$-truncation. Therefore, the model space is truncated in a global way that does not account for the physical features of the Hamiltonian and the eigenstate we are interested in. It thus contains a significant number of basis states that contribute only with vanishing or very small amplitudes C_ν to the basis expansion of the target eigenstate (4.2).

The idea of the importance truncation is to classify the basis states as important or negligible for the basis expansion of the target eigenstate $|\Psi\rangle$ without actually solving the eigenvalue problem in the full model space. For this purpose, we define an importance measure derived in the framework of multi-configurational perturbation theory to assess the relevance of the individual basis states for the description of the target eigenstate using the information provided by the Hamiltonian: We estimate the amplitudes C_ν in the basis expansion of the eigenstate $|\Psi\rangle$ using the first-order perturbative correction of an initial approximation for the target state as an importance measure. We include only basis states with an importance measure larger than a given importance threshold in the reduced, so-called importance-truncated model space. This model space is therefore tailored to the description of the target eigenstate. By solving the eigenvalue problem in the importance-truncated model space, we have to deal with significantly smaller dimensions than in the full model space while leaving the results almost unchanged. We obtain a variational approximation to the eigenstate computed in a full calculation, where the importance threshold is the control parameter.

4.2. Multi-Configurational Perturbation Theory

We start from a full model space $\mathcal{M}_{\text{full}}$ spanned by a set of basis states $|\Phi_\nu\rangle$. Furthermore, we assume a reference state $|\Psi_{\text{ref}}\rangle$, an eigenstate of the Hamiltonian $\mathbf{H}$ obtained

in a subspace $\mathcal{M}_{\text{ref}}$ of the full model space,

$$\mathbf{O}^\dagger\mathbf{H}\mathbf{O}\,|\Psi_{\text{ref}}\rangle = \epsilon_{\text{ref}}\,|\Psi_{\text{ref}}\rangle \qquad \text{with} \qquad \mathbf{O} = \sum_{\nu\in\mathcal{M}_{\text{ref}}} |\Phi_\nu\rangle\,\langle\Phi_\nu|\,, \tag{4.3}$$

$$|\Psi_{\text{ref}}\rangle = \sum_{\nu\in\mathcal{M}_{\text{ref}}} C_\nu^{(\text{ref})}\,|\Phi_\nu\rangle\,, \tag{4.4}$$

to be a zeroth-order approximation for the eigenstate of the Hamiltonian we are interested in. In the case of the shell model, the reference state is an eigenstate of a shell-model calculation in a feasible model space, e.g. the ground state computed in a truncated valence space with $T_{\text{max}} = 4$. We employ low-order multi-configurational perturbation theory to estimate the leading corrections to $|\Psi_{\text{ref}}\rangle$ resulting from basis states outside the reference space.

We split the Hamiltonian $\mathbf{H}$ into an unperturbed part $\mathbf{H}_0$ and a perturbation $\mathbf{W}$:

$$\mathbf{H} = \mathbf{H}_0 + \mathbf{W}. \tag{4.5}$$

The eigenvalue problem of the unperturbed Hamiltonian is

$$\mathbf{H}_0\,|\Psi_{\text{ref}}\rangle = \epsilon_{\text{ref}}\,|\Psi_{\text{ref}}\rangle\,, \qquad \epsilon_{\text{ref}} = \langle\Psi_{\text{ref}}|\mathbf{H}|\Psi_{\text{ref}}\rangle\,, \tag{4.6}$$

where the eigenvalue ϵ_{ref} is given by the expectation value of the full Hamiltonian with respect to the reference state. We define the unperturbed Hamiltonian so that it fulfills the eigenvalue relation (4.6):

$$\mathbf{H}_0 = \epsilon_{\text{ref}}\,|\Psi_{\text{ref}}\rangle\,\langle\Psi_{\text{ref}}| + \sum_{\nu\notin\mathcal{M}_{\text{ref}}} \epsilon_\nu\,|\Phi_\nu\rangle\,\langle\Phi_\nu|\,. \tag{4.7}$$

Eigenstates of $\mathbf{H}_0$ within $\mathcal{M}_{\text{ref}}$ that are orthogonal to $|\Psi_{\text{ref}}\rangle$ do not contribute to the energy and state corrections (see Appendix A) and are thus omitted for simplicity. Since the partitioning of the Hamiltonian is arbitrary, there are different possibilities for the choice of the eigenenergies ϵ_ν of the basis states outside $\mathcal{M}_{\text{ref}}$. As our main concern is computational feasibility, we use the simple Møller-Plesset type formulation of multi-configurational perturbation theory [33]. In this formulation, the eigenenergies of the basis states outside $\mathcal{M}_{\text{ref}}$ are defined as excitation energies with respect to the reference state:

$$\epsilon_\nu = \epsilon_{\text{ref}} + \Delta\epsilon_\nu. \tag{4.8}$$

The excitation energy $\Delta\epsilon_\nu$ is computed from the single-particle energies of the valence nucleons according to their configuration $|\Phi_\nu\rangle$. The choice of the unperturbed

Hamiltonian defines the perturbation

$$\mathbf{W} = \mathbf{H} - \mathbf{H}_0. \tag{4.9}$$

In the following, we derive the lowest-order corrections to the unperturbed eigenvalue ϵ_{ref} and eigenstate $|\Psi_{\text{ref}}\rangle$: We assume that the perturbation $\mathbf{W}$ can be controlled by a parameter λ,

$$\mathbf{H} = \mathbf{H}_0 + \lambda \mathbf{W}, \tag{4.10}$$

and that the target eigenvalue E and eigenstate $|\Psi\rangle$ can be expanded in terms of a power series in this parameter:

$$E = \epsilon_{\text{ref}} + \lambda E^{(1)} + \lambda^2 E^{(2)} + \dots , \tag{4.11}$$

$$|\Psi\rangle = |\Psi_{\text{ref}}\rangle + \lambda \, |\Psi^{(1)}\rangle + \lambda^2 \, |\Psi^{(2)}\rangle \dots . \tag{4.12}$$

By inserting the Equations (4.10) to (4.12) into (4.1), we obtain

$$\begin{aligned} \mathbf{H} \, |\Psi\rangle &= (\mathbf{H}_0 + \lambda \mathbf{W}) \left(|\Psi_{\text{ref}}\rangle + \lambda \, |\Psi^{(1)}\rangle + \lambda^2 \, |\Psi^{(2)}\rangle \dots \right) \\ &= \left(\epsilon_{\text{ref}} + \lambda E^{(1)} + \lambda^2 E^{(2)} + \dots \right) \left(|\Psi_{\text{ref}}\rangle + \lambda \, |\Psi^{(1)}\rangle + \lambda^2 \, |\Psi^{(2)}\rangle \dots \right), \end{aligned} \tag{4.13}$$

which yields the unperturbed eigenvalue problem in the limit of vanishing λ and the exact one if evaluated at $\lambda = 1$. We expand Equation (4.13) and arrange the terms according to the power of λ. The zeroth order reproduces the unperturbed eigenvalue problem (4.6). For the first-order terms, we obtain the following relation:

$$\mathbf{H}_0 \, |\Psi^{(1)}\rangle + \mathbf{W} \, |\Psi_{\text{ref}}\rangle = \epsilon_{\text{ref}} \, |\Psi^{(1)}\rangle + E^{(1)} \, |\Psi_{\text{ref}}\rangle \, . \tag{4.14}$$

We derive the first-order energy correction by multiplying (4.14) by $\langle \Psi_{\text{ref}}|$:

$$\langle \Psi_{\text{ref}}|\mathbf{H}_0|\Psi^{(1)}\rangle + \langle \Psi_{\text{ref}}|\mathbf{W}|\Psi_{\text{ref}}\rangle = \epsilon_{\text{ref}} \, \langle \Psi_{\text{ref}}|\Psi^{(1)}\rangle + E^{(1)} \, \langle \Psi_{\text{ref}}|\Psi_{\text{ref}}\rangle \, . \tag{4.15}$$

For convenience, we introduce the intermediate normalization

$$\langle \Psi_{\text{ref}}|\Psi\rangle = 1, \tag{4.16}$$

$$\langle \Psi_{\text{ref}}|\Psi^{(p>0)}\rangle = 0, \tag{4.17}$$

where p denotes the order of the perturbative correction. The first term in Equation (4.15) vanishes because $\mathbf{H}_0$ is hermitian and can be applied to $|\Psi_{\text{ref}}\rangle$. Then, the

intermediate normalization (4.17) can be used:

$$\langle \Psi_{\text{ref}} | \mathbf{H}_0 | \Psi^{(1)} \rangle = \epsilon_{\text{ref}} \langle \Psi_{\text{ref}} | \Psi^{(1)} \rangle = 0. \tag{4.18}$$

Thus, the first-oder energy correction is given by

$$E^{(1)} = \langle \Psi_{\text{ref}} | \mathbf{W} | \Psi_{\text{ref}} \rangle = 0 \tag{4.19}$$

as a consequence of the definition of $\mathbf{H}_0$. In particular,

$$\begin{aligned} \langle \Phi_\nu | \mathbf{W} | \Psi_{\text{ref}} \rangle &= \langle \Phi_\nu | \mathbf{O}^\dagger \mathbf{H} \mathbf{O} | \Psi_{\text{ref}} \rangle - \langle \Phi_\nu | \mathbf{O}^\dagger \mathbf{H}_0 \mathbf{O} | \Psi_{\text{ref}} \rangle \\ &= \epsilon_{\text{ref}} \langle \Phi_\nu | \Psi_{\text{ref}} \rangle - \epsilon_{\text{ref}} \langle \Phi_\nu | \Psi_{\text{ref}} \rangle \\ &= 0 \end{aligned} \tag{4.20}$$

holds for all $|\Phi_\nu\rangle \in \mathcal{M}_{\text{ref}}$.

By comparing the coefficients of the second order in λ of (4.13) and proceeding analogously to the derivation of $E^{(1)}$, we obtain the second-order energy correction:

$$E^{(2)} = \langle \Psi_{\text{ref}} | \mathbf{W} | \Psi^{(1)} \rangle . \tag{4.21}$$

For the computation of $E^{(2)}$, we need to know the first-order state correction $|\Psi^{(1)}\rangle$. We can expand $|\Psi^{(1)}\rangle$ in terms of the basis states of the full model space:

$$|\Psi^{(1)}\rangle = \sum_{\nu \in \mathcal{M}_{\text{full}}} |\Phi_\nu\rangle \langle \Phi_\nu | \Psi^{(1)} \rangle . \tag{4.22}$$

The coefficient $\langle \Phi_\nu | \Psi^{(1)} \rangle$ can be determined by multiplying (4.14) by $\langle \Phi_\nu |$:

$$\begin{aligned} \langle \Phi_\nu | \mathbf{H}_0 | \Psi^{(1)} \rangle + \langle \Phi_\nu | \mathbf{W} | \Psi_{\text{ref}} \rangle &= \epsilon_{\text{ref}} \langle \Phi_\nu | \Psi^{(1)} \rangle + E^{(1)} \langle \Phi_\nu | \Psi_{\text{ref}} \rangle \\ &= \epsilon_{\text{ref}} \langle \Phi_\nu | \Psi^{(1)} \rangle . \end{aligned} \tag{4.23}$$

In the following, we consider basis states $|\Phi_\nu\rangle$ belonging to the reference space and basis states outside the reference space separately:

- $|\Phi_\nu\rangle \in \mathcal{M}_{\text{ref}}$:
  We insert (4.7) into the first term of (4.23):

$$\langle \Phi_\nu | \mathbf{H}_0 | \Psi^{(1)} \rangle = \epsilon_{\text{ref}} \langle \Phi_\nu | \Psi_{\text{ref}} \rangle \langle \Psi_{\text{ref}} | \Psi^{(1)} \rangle + \sum_{\mu \notin \mathcal{M}_{\text{ref}}} \epsilon_\mu \langle \Phi_\nu | \Phi_\mu \rangle \langle \Phi_\mu | \Psi^{(1)} \rangle = 0. \tag{4.24}$$

We have used the intermediate normalization (4.17) and the fact that basis states of orthogonal spaces do not overlap. The second term of (4.23) vanishes because of (4.20) and therefore we have

$$\langle \Phi_\nu | \Psi^{(1)} \rangle = 0 \qquad \forall\ |\Phi_\nu\rangle \in \mathcal{M}_{\text{ref}}. \tag{4.25}$$

Hence, basis states of the reference space do not contribute to the basis expansion of the first-order correction to the eigenstate.

- $|\Phi_\nu\rangle \notin \mathcal{M}_{\text{ref}}$:
  In this case, the first term yields

$$\begin{aligned}
\langle \Phi_\nu | \mathbf{H}_0 | \Psi^{(1)} \rangle &= \epsilon_{\text{ref}} \langle \Phi_\nu | \Psi_{\text{ref}} \rangle \langle \Psi_{\text{ref}} | \Psi^{(1)} \rangle + \sum_{\mu \notin \mathcal{M}_{\text{ref}}} \epsilon_\mu \langle \Phi_\nu | \Phi_\mu \rangle \langle \Phi_\mu | \Psi^{(1)} \rangle && (4.26)\\
&= \sum_{\mu \notin \mathcal{M}_{\text{ref}}} \epsilon_\mu \langle \Phi_\nu | \Phi_\mu \rangle \langle \Phi_\mu | \Psi^{(1)} \rangle && (4.27)\\
&= \epsilon_\nu \langle \Phi_\nu | \Psi^{(1)} \rangle && (4.28)
\end{aligned}$$

  and Equation (4.23) reduces to

$$\epsilon_\nu \langle \Phi_\nu | \Psi^{(1)} \rangle + \langle \Phi_\nu | \mathbf{W} | \Psi_{\text{ref}} \rangle = \epsilon_{\text{ref}} \langle \Phi_\nu | \Psi^{(1)} \rangle . \tag{4.29}$$

  Rewriting this relation gives the coefficient $\langle \Phi_\nu | \Psi^{(1)} \rangle$ for basis states $|\Phi_\nu\rangle$ outside the reference space:

$$\langle \Phi_\nu | \Psi^{(1)} \rangle = -\frac{\langle \Phi_\nu | \mathbf{W} | \Psi_{\text{ref}} \rangle}{\epsilon_\nu - \epsilon_{\text{ref}}} \qquad \forall\ |\Phi_\nu\rangle \notin \mathcal{M}_{\text{ref}}. \tag{4.30}$$

The first-order state correction is then given by

$$\begin{aligned}
|\Psi^{(1)}\rangle &= \sum_{\nu \notin \mathcal{M}_{\text{ref}}} -\frac{\langle \Phi_\nu | \mathbf{W} | \Psi_{\text{ref}} \rangle}{\epsilon_\nu - \epsilon_{\text{ref}}} |\Phi_\nu\rangle && (4.31)\\
&= \sum_{\nu \notin \mathcal{M}_{\text{ref}}} -\frac{\langle \Phi_\nu | \mathbf{H} | \Psi_{\text{ref}} \rangle}{\epsilon_\nu - \epsilon_{\text{ref}}} |\Phi_\nu\rangle , && (4.32)
\end{aligned}$$

where we have used the fact that matrix elements of the unperturbed Hamiltonian between the reference state $|\Psi_{\text{ref}}\rangle$ and the basis states $|\Phi_\nu\rangle \notin \mathcal{M}_{\text{ref}}$ vanish by construction, see Equation (4.20). Inserting the basis expansion of $|\Psi^{(1)}\rangle$ into (4.21), we obtain

$$E^{(2)} = -\sum_{\nu \notin \mathcal{M}_{\text{ref}}} \frac{\left| \langle \Phi_\nu | \mathbf{W} | \Psi_{\text{ref}} \rangle \right|^2}{\epsilon_\nu - \epsilon_{\text{ref}}} \tag{4.33}$$

$$= - \sum_{\nu \notin \mathcal{M}_{\text{ref}}} \frac{|\langle \Phi_\nu | \mathbf{H} | \Psi_{\text{ref}} \rangle|^2}{\epsilon_\nu - \epsilon_{\text{ref}}}. \tag{4.34}$$

In the following, we summarize the relations for the lowest-order energy and state corrections:

$$\boxed{\begin{aligned} E^{(0)} &= \epsilon_{\text{ref}}, && (4.35)\\ E^{(1)} &= \langle \Psi_{\text{ref}} | \mathbf{W} | \Psi_{\text{ref}} \rangle = 0, && (4.36)\\ E^{(2)} &= - \sum_{\nu \notin \mathcal{M}_{\text{ref}}} \frac{|\langle \Phi_\nu | \mathbf{H} | \Psi_{\text{ref}} \rangle|^2}{\epsilon_\nu - \epsilon_{\text{ref}}}, && (4.37) \end{aligned}}$$

$$\boxed{\begin{aligned} |\Psi^{(0)}\rangle &= |\Psi_{\text{ref}}\rangle\,, && (4.38)\\ |\Psi^{(1)}\rangle &= \sum_{\nu \notin \mathcal{M}_{\text{ref}}} - \frac{\langle \Phi_\nu | \mathbf{H} | \Psi_{\text{ref}} \rangle}{\epsilon_\nu - \epsilon_{\text{ref}}} |\Phi_\nu\rangle\,. && (4.39) \end{aligned}}$$

4.3. Importance Measure

The main goal of the importance-truncation scheme is to assess the relevance of individual basis states $|\Phi_\nu\rangle$ *a priori* for the basis expansion of one or a few target eigenstates, i.e. without solving the eigenvalue problem of the nuclear Hamiltonian in the full model space. The target eigenstate is initially approximated by a reference state $|\Psi_{\text{ref}}\rangle \in \mathcal{M}_{\text{ref}}$ carrying the correct quantum numbers. In the shell model, the reference state is given by the eigenstate obtained in a shell-model calculation in a subspace of the valence space. We use multi-configurational perturbation theory to estimate the importance of basis states outside the reference space $|\Phi_\nu\rangle \notin \mathcal{M}_{\text{ref}}$ for the basis expansion of the target eigenstate in the full model space $\mathcal{M}_{\text{full}}$: We employ the amplitude of the basis states in the basis expansion of the first-order state correction (4.39) as dimensionless importance measure:

$$\boxed{\begin{aligned} \kappa_\nu &= - \frac{\langle \Phi_\nu | \mathbf{H} | \Psi_{\text{ref}} \rangle}{\epsilon_\nu - \epsilon_{\text{ref}}} && (4.40)\\ &= - \sum_{\mu \in \mathcal{M}_{\text{ref}}} C_\mu^{(\text{ref})} \frac{\langle \Phi_\nu | \mathbf{H} | \Phi_\mu \rangle}{\epsilon_\nu - \epsilon_{\text{ref}}}. && (4.41) \end{aligned}}$$

Basis states with an importance measure $|\kappa_\nu|$ larger than a given importance threshold κ_{min} are used to construct the importance-truncated model space $\mathcal{M}_{\text{IT}}(\kappa_{\text{min}})$. In this way, we obtain a reduced model space tailored to a particular Hamiltonian and target eigenstate. The dimension of the importance-truncated model space can be controlled via the importance threshold κ_{min}. In the limit of vanishing importance threshold, $\kappa_{\text{min}} \to 0$, the full model space is recovered.

An alternative importance measure can be derived from the second-order energy

correction (4.37):

$$\boxed{\xi_\nu = -\frac{\left|\langle\Phi_\nu|\mathbf{H}|\Psi_{\mathrm{ref}}\rangle\right|^2}{\epsilon_\nu - \epsilon_{\mathrm{ref}}}.} \tag{4.42}$$

This importance measure characterizes the relevance of the basis states outside the reference space for the computation of the energy. As we are interested in an optimum description of the target eigenstate, from which we can compute the expectation value of the energy and other observables, we employ the state-based importance measure κ_ν (4.41).

In the case of a two-body Hamiltonian, the importance measure κ_ν connects only basis states that differ by two single-particle states at most from the reference state (two-particle two-hole (2p2h) excitations) and vanishes otherwise. If we start from a reference state obtained in a shell-model calculation in a valence space with $T_{\mathrm{max}} = 4$ truncation, we can only add up to 2p2h excitations on top of the reference state to the importance-truncated model space yielding at most $T_{\mathrm{max}} = 6$ states. To access up to 4p4h excitations, we need to consider the amplitudes of the second-order correction in multi-configurational perturbation theory to the reference state. But the evaluation of higher orders in multi-configurational perturbation theory is computationally demanding. Therefore, we embed the importance measure κ_ν in an iterative scheme to construct the importance-truncated model space for larger T_{max}.

The procedure described above generalizes to the simultaneous description of a few eigenstates: We start from a set of reference states $|\Psi_{\mathrm{ref}}^{(n)}\rangle$, e.g. some low-lying eigenstates of the Hamiltonian in a small valence space with T_{max}-truncation. We construct separate importance measures $\kappa_\nu^{(n)}$ for each of the reference states and include a basis state $|\Phi_\nu\rangle$ in the importance-truncated model space if one of the importance measures $\left|\kappa_\nu^{(n)}\right|$ exceeds the importance threshold. That way, one obtains a combined model space tailored to the simultaneous description of all target eigenstates.

4.4. Iterative Model-Space Construction

Since the importance measure κ_ν (4.41) can only be used to extend the reference space to basis states of up to 2p2h excitations on top of the reference state, it is embedded into an iterative scheme to construct the importance-truncated model space for a given importance threshold κ_{min}. The iteration is illustrated in Figure 4.1: We start from an initial approximation for the target state, e.g. an eigenstate of a shell-model calculation in a valence space $\mathcal{M}_{\mathrm{ref}}$ with $T_{\mathrm{max}} = 4$ truncation. This state is used as reference state $|\Psi_{\mathrm{ref}}\rangle$ in the first iteration. We employ the importance measure κ_ν to the basis states outside $\mathcal{M}_{\mathrm{ref}}$ to construct all 1p1h and 2p2h excitations of $|\Psi_{\mathrm{ref}}\rangle$ and include those

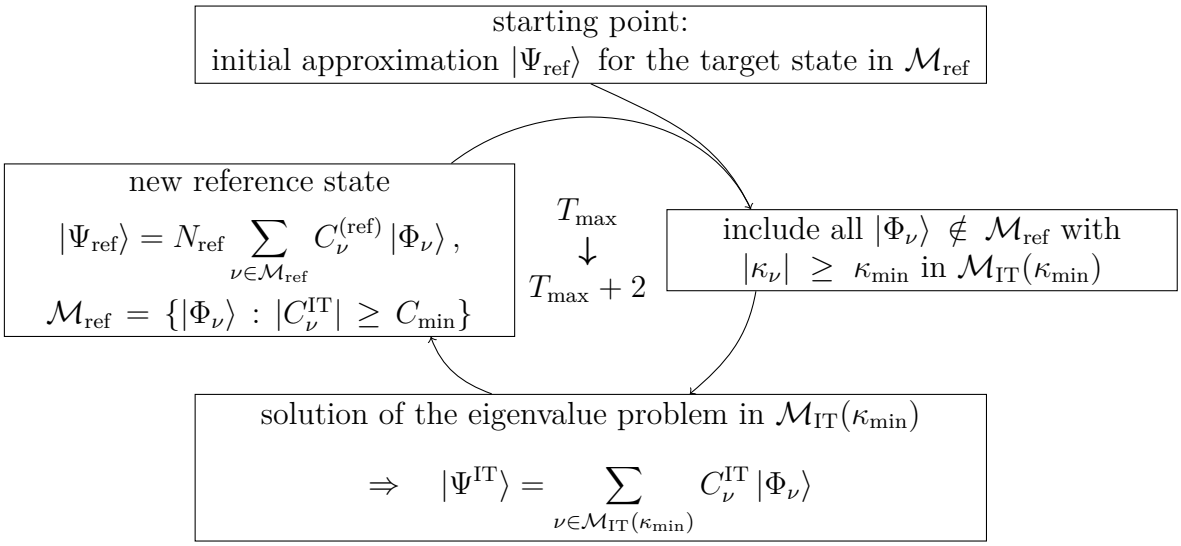

Figure 4.1.: Iterative model-space construction.

with $|\kappa_\nu| \geq \kappa_{\text{min}}$ in the importance-truncated, now $T_{\text{max}} = 6$, valence space $\mathcal{M}_{\text{IT}}(\kappa_{\text{min}})$. By solving the eigenvalue problem within this new model space, we obtain an eigenstate which is an improved approximation for the target state:

$$|\Psi^{\text{IT}}\rangle = \sum_{\nu\in\mathcal{M}_{\text{IT}}(\kappa_{\text{min}})} C_\nu^{\text{IT}} |\Phi_\nu\rangle\,. \tag{4.43}$$

We could use $|\Psi^{\text{IT}}\rangle$ directly as reference state for the next iteration, but in order to accelerate the evaluation of the importance measure, we first project it onto a new reference space $\mathcal{M}_{\text{ref}}$ spanned by the basis states $|\Phi_\nu\rangle \in \mathcal{M}_{\text{IT}}(\kappa_{\text{min}})$ with amplitudes $|C_\nu^{\text{IT}}| \geq C_{\text{min}}$. Hence, the reference state for the second iteration is given by

$$|\Psi_{\text{ref}}\rangle = N_{\text{ref}} \sum_{\nu\in\mathcal{M}_{\text{ref}}} C_\nu^{(\text{ref})} |\Phi_\nu\rangle\,, \tag{4.44}$$

with a normalization constant N_{ref}. The coefficients $C_\nu^{(\text{ref})}$ are the coefficients in the basis expansion of the eigenstate $|\Psi^{\text{IT}}\rangle$ which exceed the reference threshold. Again, we apply the importance measure to construct up to 2p2h excitations on top of the reference state $|\Psi_{\text{ref}}\rangle$. In total, we have built basis states that differ by up to four single-particle states from the original reference state ($T_{\text{max}} = 8$). By repeating the previous steps, the importance-truncated valence space is constructed. In each iteration, the basis states are reassessed with respect to their relevance for the description of the target eigenstate using the most recent reference state. In this way, the coupling of basis states with lower $np n$h excitations to basis states with higher orders of $np n$h

excitations is accounted for in the importance-truncated valence space.

4.5. *A posteriori* Correction to the Energy

The eigenenergies $E(\kappa_{\min})$ obtained in IT-SM calculations are approximations to the exact energies since they are computed from a subset of basis states of the complete valence space. We define corrections to the energies $E(\kappa_{\min})$ which result from configurations not included in the importance-truncated valence space because their importance measure is below the threshold $\kappa_{\min}$.

We apply the sum of the second-order energy corrections (4.37) of the excluded states as approximate measure for the contribution of basis states with $|\kappa_\nu| < \kappa_{\min}$ to the exact energy:

$$\Delta_{\mathrm{excl}}(\kappa_{\min}) = -\sum_{\nu \notin \mathcal{M}_{\mathrm{IT}}(\kappa_{\min})} \frac{\left|\langle \Phi_\nu | \mathbf{H} | \Psi_{\mathrm{ref}} \rangle\right|^2}{\epsilon_\nu - \epsilon_{\mathrm{ref}}}. \tag{4.45}$$

The evaluation of this energy correction poses no additional computational effort since the matrix elements are computed anyway for the evaluation of the importance measure κ_ν. Thus, this energy correction can be taken as a by-product of the construction of the importance-truncated valence space. It is an approximation for the effect of excluded Slater determinants on the energy because only the coupling to the reference state and not the recently processed basis states of the reference space are accounted for.

However, this *a posteriori* correction to the energy $E(\kappa_{\min})$ exhibits the property to vanish in the limit $\kappa_{\min} \to 0$. We exploit this feature in order to stabilize the threshold extrapolation, see Section 4.8.

The corrected energies are then given by

$$\tilde{E}(\kappa_{\min}) = E(\kappa_{\min}) + \Delta_{\mathrm{excl}}(\kappa_{\min}). \tag{4.46}$$

4.6. Characteristics of the Importance-Truncated Shell Model

In the following, we specify a few general characteristics of the IT-SM which do not depend on a given nucleus or valence space: The IT-SM is a strictly variational approach to the conventional shell model. The energies are determined by solving the eigenvalue problem in a reduced valence space, where the smallest eigenvalue provides an upper bound for the exact energy. Furthermore, the Hylleraas-Undheim theorem [34] applies,

i.e. the energy of all states is guaranteed to drop monotonically with decreasing $\kappa_{\min}$ and reaches its exact value for the full valence space:

$$E_{\text{exact}} \leq E(\kappa_{\min}) \leq E(\kappa'_{\min}) \text{ for } \kappa_{\min} < \kappa'_{\min}. \tag{4.47}$$

Since the full valence space is recovered in the limit of vanishing thresholds ($\kappa_{\min} \to 0$, $C_{\min} \to 0$), extrapolations to $\kappa_{\min} = 0$ are used in practice and give an approximate result for the full valence space.

4.7. Implementation

The implementation of the IT-SM code differs from the conventional shell-model code in the construction of the model space. In the conventional shell model, the model space is spanned by all possible Slater determinants built from the single-particle states of the valence nucleons that carry the correct quantum numbers. In the IT-SM, the model space contains only those basis states which are relevant for the basis expansion of one or a few target eigenstates. The subsequent computation and diagonalization of the Hamilton matrix does not require any modifications of the code. Since the model-space dimension is reduced by typically at least two orders of magnitude in the IT-SM, this part of the calculation is computationally much less demanding than in the conventional shell model.

We construct the importance-truncated valence space iteratively startig from a given reference state $|\Psi_{\text{ref}}\rangle$. In the first iteration, $|\Psi_{\text{ref}}\rangle$ is given by the solution of the eigenvalue problem of the Hamiltonian in a small, truncated valence space, e.g. with $T_{\max} = 2$ or $T_{\max} = 4$. In subsequent iterations, we employ the eigenstate of the Hamiltonian in an importance-truncated model space as reference state. The reference space $\mathcal{M}_{\text{ref}}$ contains those basis states which contribute with an amplitude larger than a reference threshold $C_{\min}$ to the basis expansion of $|\Psi_{\text{ref}}\rangle$. We loop over all basis states $|\Phi_\nu\rangle \in \mathcal{M}_{\text{ref}}$ and create all 1p1h and 2p2h excitations $|\Phi_\mu\rangle$ on top of each basis state. We compare $|\Phi_\mu\rangle$ to all previously processed basis states. If it is no duplicate of an already considered basis state, the importance measure (4.41) is evaluated. The basis state $|\Phi_\mu\rangle$ is included in the importance-truncated valence space $\mathcal{M}_{\text{IT}}(\kappa_{\min})$ if its importance measure exceeds $\kappa_{\min}$.

Evidently, the cost for an update of the importance-truncated valence space grows quadratically with the number of basis states in $\mathcal{M}_{\text{ref}}$.

Since we only include basis states with $|C_\nu^{\text{IT}}| \geq C_{\min}$ in $\mathcal{M}_{\text{ref}}$ in order to accelerate the model-space construction, we always check if a variation of the reference threshold $C_{\min}$ has sizeable effects on the results. We chose $C_{\min}$ to be of the order of 10^{-4}

yielding reference spaces composed of typically up to 10^6 basis states.

As the result of each iteration, we obtain an importance-truncated valence space including the importance measures of the basis states. Each iteration corresponds to a different IT-SM calculation starting from a reference state obtained in a previous shell-model or IT-SM calculation. In each iteration, the maximum particle-hole truncation $T_{\max}$ increases by two. The iteration is carried out until the eigenvalues converge with respect to $T_{\max}$. In the case of the maximum value for $T_{\max} = A_{\mathrm{val}}$, we obtain the importance-truncated valence space corresponding to the full valence space.

The eigenvalue problem is eventually solved in this importance-truncated model space. The eigenstates are given in the usual shell-model representation and we can use them to compute expectation values of observables.

4.8. Threshold Dependence and Extrapolation

An efficient probe for the quality of an IT-SM calculation is the variation of the threshold $\kappa_{\min}$. Furthermore, this variation provides the basis for an extrapolation to vanishing importance threshold, which accounts approximately for the effects of excluded configurations. Therefore, we evaluate the results of an IT-SM calculation in the following way: We perform a sequence of IT-SM calculations for different values of $\kappa_{\min}$. Each $\kappa_{\min}$ corresponds to a particular importance-truncated valence space for which the eigenvalue problem has to be solved. We apply a filtering method in order to minimize the computational cost: We construct the importance-truncated valence space and Hamilton matrix for the smallest $\kappa_{\min}$ of the sequence and solve the eigenvalue problem in this model space. In order to access the next-lowest $\kappa'_{\min}$, we remove those basis states $|\Phi_\nu\rangle$ that do not fulfill the condition $|\kappa_\nu| \geq \kappa'_{\min}$ any more from the importance-truncated valence space and the corresponding columns and rows from the Hamilton matrix. The remaining basis states span the importance-truncated valence space corresponding to the current threshold $\kappa'_{\min}$, in which the eigenvalue problem is solved again. This procedure is repeated until the largest $\kappa_{\min}$ of the sequence has been addressed. In this way, we construct the computationally demanding and time-consuming importance-truncated valence space and Hamilton matrix only once per $\kappa_{\min}$-sequence.

Figure 4.2 (a) depicts the threshold dependence of the energy with and without perturbative correction, $\tilde{E}(\kappa_{\min})$ and $E(\kappa_{\min})$, respectively. The energy eigenvalue $E(\kappa_{\min})$ decreases monotonically with decreasing $\kappa_{\min}$, as expected from the variational principle. The importance-truncated valence-space dimension increases with decreasing $\kappa_{\min}$, see Figure 4.2 (b). The most relevant configurations for the description of the

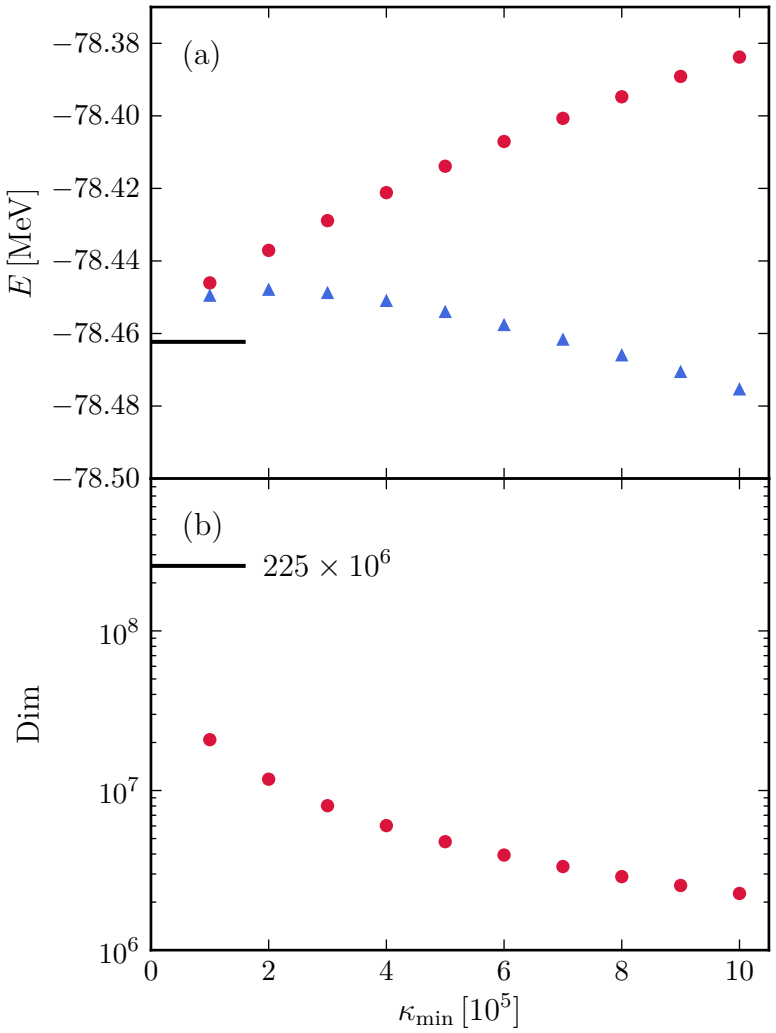

Figure 4.2.: IT-SM calculation for ^{56}Ni with $T_{\max} = 8$ and $C_{\min} = 10^{-4}$ using the KB3 interaction [35]. (a) Threshold dependence of the ground-state energy $E(\kappa_{\min})$ (●) and the ground-state energy with perturbative corrections $\tilde{E}(\kappa_{\min})$ (▲). The exact value computed with the ANTOINE code [36] is plotted as a solid line. (b) Threshold dependence of the dimension of the importance-truncated valence space constructed for the simultaneous description of six eigenstates. For comparison, the corresponding model-space dimension of a conventional shell-model calculation for the same $T_{\max}$ is indicated (solid line).

target eigenstates have large importance measures, and are already included in the importance-truncated model space for large values of $\kappa_{\min}$. For decreasing $\kappa_{\min}$, progressively less important basis states are included. They are numerous, but their effect on the eigenstates and eigenenergies is moderate. Since the perturbative energy correction (4.45) accounts already approximately for excluded configurations, $\tilde{E}(\kappa_{\min})$ shows a weaker threshold dependence than $E(\kappa_{\min})$. But we have only included the second-order perturbative energy corrections and have neglected the higher orders of the perturbation series. Thus, the approximation is not perfect and becomes worse for smaller importance-truncated valence spaces, i.e. larger values of $\kappa_{\min}$, and gives rise to an overbinding of the ground state. For the three smallest values of $\kappa_{\min}$, $\tilde{E}(\kappa_{\min})$ has almost no threshold dependence. In the limit $\kappa_{\min} \to 0$, the corrections vanish and the energy $E(\kappa_{\min}) = \tilde{E}(\kappa_{\min})$ becomes exact.

Since the eigenenergy $E(\kappa_{\min})$ is a smooth and monotonous function of $\kappa_{\min}$, we fit a polynomial $P^{(n)}(\kappa_{\min})$, typically of the order three or four, to a sufficiently large number of energies E for different values of $\kappa_{\min}$. The fitted curve evaluated at $\kappa_{\min} = 0$ represents the extrapolated energy $E(\kappa_{\min} = 0)$. In order to estimate the accuracy of the extrapolation, we define an error band for the fitted energy function: We fit two polynomials $P^{(n-1)}(\kappa_{\min})$ and $P^{(n+1)}(\kappa_{\min})$ to the $\kappa_{\min}$-sequence. Additionally, we fit the polynomial $P^{(n)}(\kappa_{\min})$ to the function $E(\kappa_{\min})$ omitting the first and the first two data points of E. Then, we determine the maximum and minimum curves resulting from the five fits as error bands. In Figure 4.3, we show the ground-state energy of ^{56}Ni obtained in an IT-SM calculation, which is a smooth function of $\kappa_{\min}$. Consequently, the fits are precise and the error bands extremely narrow. The nominal error of the energy $E(\kappa_{\min} = 0)$ is given by the standard deviation of the five extrapolations at $\kappa_{\min} = 0$.

We apply the same extrapolation technique in order to account for excluded configurations when computing observables although the variational principle does not hold true in these cases, see Section 6.1.2.

A more elaborate threshold extrapolation for the energy can be carried out by defining a set of energy functions

$$\tilde{E}_\lambda(\kappa_{\min}) = E(\kappa_{\min}) + \lambda \Delta_{\text{excl}}(\kappa_{\min}). \tag{4.48}$$

The extrapolations of the functions $\tilde{E}_\lambda(\kappa_{\min})$ should give the same value for the energy at $\kappa_{\min} = 0$ independently of the parameter λ because the energy correction $\Delta_{\text{excl}}(\kappa_{\min})$ vanishes in the limit $\kappa_{\min} \to 0$. We fit polynomials $P^{(n)}(\kappa_{\min})$ to $\tilde{E}_\lambda(\kappa_{\min})$ for typically five different values for λ under the constraint that all $\tilde{E}_\lambda(\kappa_{\min})$ must have the same value at $\kappa_{\min} = 0$. In this way, we reduce the uncertainty of the extrapolation. This

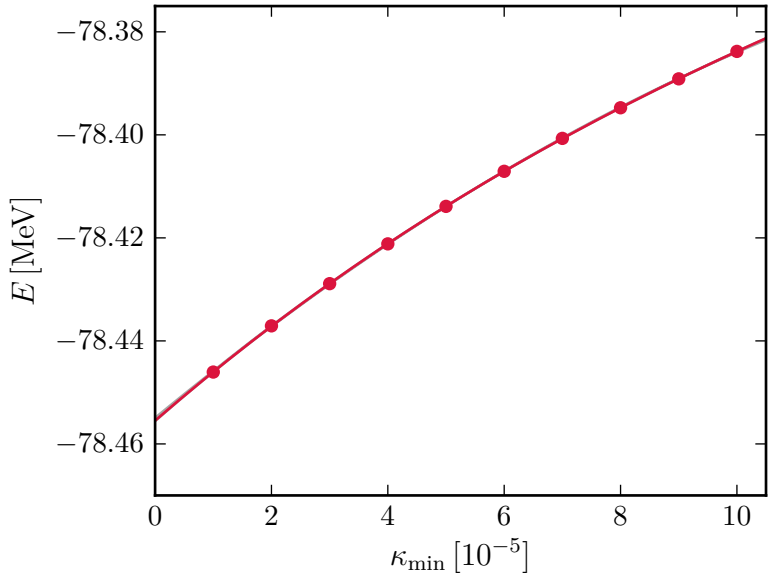

Figure 4.3.: Threshold extrapolation with error bands for the ground-state energy $E(0_1^+)$ of ^{56}Ni computed in an IT-SM calculation with $T_{\max} = 8$ and $C_{\min} = 10^{-4}$ using the KB3 interaction.

simultaneous threshold-extrapolation technique was also applied in quantum chemistry [37], where the only requirement is a monotonous and smooth perturbative correction $\Delta_{\text{excl}}(\kappa_{\min})$ which vanishes in the limit $\kappa_{\min} \to 0$. It provides more stable results than the simple extrapolation technique and can therefore be applied as a cross-check for the latter. Evidently, the constrained threshold extrapolations are most stable if the energies $\tilde{E}_\lambda(\kappa_{\min})$ approach $\kappa_{\min} = 0$ symmetrically. This is illustrated in Figure 4.4, where we show the constrained threshold extrapolation for ^{56}Ni using the parameter set $\lambda = \{0, 0.5, 1, 1.5, 2\}$. We assess the uncertainty of the constrained threshold extrapolation in the same way as for the simple extrapolation technique. Additionally, we repeat the constrained threshold extrapolation twice, omitting the energy function $\tilde{E}_\lambda(\kappa_{\min})$ with either the smallest or largest value of λ. The variance of this set of extrapolations defines an uncertainty interval for the threshold extrapolated energy.

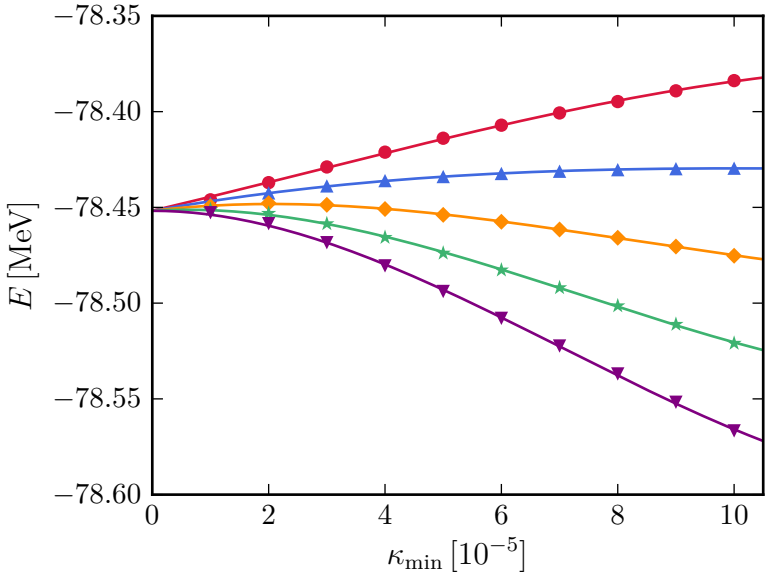

Figure 4.4.: Constrained threshold extrapolation of the perturbatively corrected ground-state energy $\tilde{E}_\lambda(\kappa_{\min})$ of ^{56}Ni obtained in an IT-SM calculation with $T_{\max} = 8$ and $C_{\min} = 10^{-4}$ using the KB3 interaction. The parameter set for λ is {0 (●), 0.5 (▲), 1 (◆), 1.5 (★), 2 (▼)}.

Chapter 5

Monte-Carlo Shell Model

The Monte-Carlo shell model (MCSM) [6] is a stochastic approach in order to overcome the limitations of the conventional shell model. As the IT-SM, it is based on the idea that a small number of important basis states of the full Hilbert space are sufficient to describe the ground state and some low-lying excited states. The quantum Monte-Carlo diagonalization [38] is applied to the nuclear shell model. In this process, the most relevant basis states for the description of one or a few eigenstates of the Hamiltonian are identified. The Hamilton matrix is constructed in a small subspace of the full Hilbert space, which is spanned by the important basis states, and is diagonalized.

Starting point of a MCSM calculation is the imaginary-time evolution operator $e^{-\beta \mathbf{H}}$ acting on an initial state $|\Psi^{(0)}\rangle$:

$$e^{-\beta \mathbf{H}} |\Psi^{(0)}\rangle = \sum_i e^{-\beta E_i} c_i |\phi_i\rangle . \tag{5.1}$$

The parameter β is a real number and $\mathbf{H}$ is the nuclear Hamiltonian. On the right-hand side of this equation, we have expanded the initial state $|\Psi^{(0)}\rangle$ in the eigenbasis $\{|\phi_i\rangle\}$ of the Hamiltonian and we have used the eigenvalue relation of the Hamiltonian. For large values of β, the excited states are progressively suppressed. In the limit $\beta \to \infty$, only the ground state survives, provided that the initial state is not orthogonal to it. Thus, the imaginary-time evolution operator acts like a projector onto the ground state for large β. We use a 2B Hamiltonian

$$\mathbf{H} = \sum_{i,j}^{N_{sp}} \epsilon_{ij} \mathbf{c}_i^\dagger \mathbf{c}_j + \frac{1}{4} \sum_{i,j,k,l}^{N_{sp}} v_{ijkl} \mathbf{c}_i^\dagger \mathbf{c}_j^\dagger \mathbf{c}_l \mathbf{c}_k \tag{5.2}$$

for the solution of the nuclear eigenvalue problem. The operators $\mathbf{c}_i^\dagger$ and $\mathbf{c}_i$ are the creation and annihilation operators for a nucleon in the single-particle state i, respec-

tively, and N_{sp} is the number of single-particle states in the valence space. In practice, the handling of the operator $e^{-\beta \mathbf{H}}$ is complicated because it can only be expressed as an infinite power series in $\mathbf{H}$ if the eigenbasis of the nuclear Hamiltonian is not known. As a remedy, we rewrite the Hamiltonian given in (5.2) in a quadratic form of 1B operators $\mathbf{O}_\alpha = \sum_{i,j} o_{ij}^{(\alpha)} \mathbf{c}_i^\dagger \mathbf{c}_j$:

$$\mathbf{H} = \sum_{\alpha=1}^{N_f} (E_\alpha \mathbf{O}_\alpha + \frac{1}{2} V_\alpha \mathbf{O}_\alpha^2). \tag{5.3}$$

The number of operators $\mathbf{O}_\alpha$ is denoted by N_f and can be smaller than or equal to N_{sp}^2. We divide the imaginary time β into N_t time steps $\Delta\beta = \frac{\beta}{N_t}$ and apply the Hubbard-Stratonovich transformation [39, 40] to the operator

$$e^{-\beta \mathbf{H}} = \prod_{n=1}^{N_t} e^{-\Delta\beta \mathbf{H}} \approx \int_{-\infty}^{\infty} \prod_{\alpha,n} \mathrm{d}\sigma_{\alpha,n} \left(\frac{\Delta\beta \, |V_\alpha|}{2\pi} \right)^{\frac{1}{2}} \cdot G(\sigma) \cdot \prod_n e^{-\Delta\beta h(\vec{\sigma}_n)} \tag{5.4}$$

at each time step. The so-called "auxiliary field" $\vec{\sigma}_n$ is a set of random numbers for the n-th time step, $\vec{\sigma}_n = (\sigma_{1,n}, \sigma_{2,n}, \ldots, \sigma_{N_t,n})$, and $\sigma = \{\vec{\sigma}_1, \vec{\sigma}_2, \ldots, \vec{\sigma}_{N_t}\}$ is the assembly of auxiliary fields over all time steps. The probability density function

$$G(\sigma) = e^{-\sum_{\alpha,n} \frac{\Delta\beta}{2} |V_\alpha| \sigma_{\alpha,n}^2} \tag{5.5}$$

is the Gaussian weight factor used for the random sampling of the auxiliary fields σ. The 1B Hamiltonian is given by

$$h(\vec{\sigma}_n) = \sum_\alpha \left(E_\alpha + s_\alpha V_\alpha \sigma_{\alpha,n} \right) \mathbf{O}_\alpha, \tag{5.6}$$

where $s_\alpha = \pm 1 (\pm i)$ for $V_\alpha < 0 \, (> 0)$. We approximate the integration in Equation (5.4) by a Monte-Carlo sampling over the auxiliary fields σ. If this approximation is treated with sufficient accuracy, the ground state can be obtained by applying the operator $e^{-\beta \mathbf{H}}$ given in (5.4) for large β to any initial state $|\Psi^{(0)}\rangle$ that is not orthogonal to the ground state:

$$|\Phi_g\rangle \sim \sum_{MC:\sigma} \prod_{n=1}^{N_t} e^{-\Delta\beta h(\vec{\sigma}_n)} \, |\Psi^{(0)}\rangle \, . \tag{5.7}$$

We assume that the right-hand side of this equation produces all basis states needed for the description of the ground state and construct the corresponding model space iteratively: We start from an initial state $|\Psi^{(0)}\rangle$, usually the Hartree-Fock ground state with its initial energy $E^{(0)} = \langle \Psi^{(0)} | \mathbf{H} | \Psi^{(0)} \rangle$. We determine a set of auxiliary fields σ stochastically by means of the Gaussian weight function. A trial state for an important

basis state is then given by

$$|\Phi(\sigma)\rangle \propto \prod_{n=1}^{N_t} e^{-\Delta\beta h(\vec{\sigma}_n)} |\Psi^{(0)}\rangle \,. \tag{5.8}$$

In the course of the iteration, we orthonormalize $|\Phi(\sigma)\rangle$ with respect to all previously determined basis states using the Gram-Schmidt method. Then, we construct and diagonalize the Hamilton matrix in the model space including the trial state. If the trial state $|\Phi(\sigma)\rangle$ has a sizeable effect on the energy, i.e. if the ground-state energy is lowered significantly compared to the one of the previous diagonalization, it is included into the Monte-Carlo model space and discarded otherwise. The previous steps are repeated using new sets of auxiliary fields until the ground-state energy is converged.

Thus, the solution of the eigenvalue problem reduces to the diagonalization of the Hamilton matrix in a much smaller model space than the full Hilbert space. Excited states can be assessed by first constructing the MCSM space for the ground state. When the ground-state energy has converged, we continue to probe if a trial state lowers the eigenenergy of the next-lowest eigenstate and proceed in the same way as described above.

In order to carry out large-scale shell-model calculations using the MCSM, some methodological improvements are necessary. For example, we can optimize the choice of the initial state by using the ground-state Slater determinant obtained in a Hartree-Fock calculation using the shell-model Hamiltonian $\mathbf{H}$ in the given single-particle space. Furthermore, the nucleus is subject to several symmetries such as parity and rotational invariance. The eigenstates obtained in a MCSM calculation do not perfectly fulfill these symmetries because the basis states of the small Monte-Carlo model space cannot fully accommodate for them. Therefore, these quantities need to be restored, e.g. by using projection methods. Thus, a MCSM calculation provides a sequence of approximated eigenstates, which are linear combinations of the angular-momentum and parity-projected deformed Slater determinants. Details of the MCSM and further refinements are given in [6].

In the MCSM, the convergence of the energy eigenvalue with respect to the number of basis states is often limited by computation time. Therefore, we apply the so-called sequential conjugate gradient (SCG) method [41] to the sequence of approximated eigenstates: The Monte-Carlo basis states are varied in such a way that the diagonalization of the Hamilton matrix in the modified model space minimizes the energy eigenvalue and improves the approximated eigenstates. Since a small gap between the exact energy and the energy expectation value of the approximated eigenstate remains, we carry out an energy-variance extrapolation [42]: For each target eigenstate, the SCG method

provides a sequence of approximated eigenstates $\{|\Psi_1\rangle, |\Psi_2\rangle, \ldots, |\Psi_i\rangle, \ldots, |\Psi_N\rangle\}$ specified by a set of basis states with a certain order $\{|\phi_1\rangle, |\phi_2\rangle, \ldots, |\phi_i\rangle, \ldots, |\phi_N\rangle\}$ and the corresponding eigenenergies $E_1, E_2, \ldots, E_i, \ldots, E_N$, where N is the MCSM dimension. Additionally, we evaluate the energy variance

$$\sigma_i^2 = \langle\Psi_i|\mathbf{H}^2|\Psi_i\rangle - \langle\Psi_i|\mathbf{H}|\Psi_i\rangle^2 \tag{5.9}$$

for each of these approximated eigenstates. In Figure 5.1, their energy eigenvalues are plotted versus their energy variance. For increasing i, more basis states are taken into account and the energy of the approximated eigenstates approaches the exact energy while the corresponding energy variance decreases. We fit a second-order polynomial to the energy and extrapolate to $\sigma^2 \to 0$. In some cases, the energy shows a kink if plotted versus the energy variance due to shape coexistence [42]. We therefore introduce a reordering technique [42] of the basis states in order to stabilize the extrapolation: We permute the basis states and diagonalize the Hamilton matrices constructed for each of the one- to N-dimensional Monte-Carlo model spaces. We then stabilize the extrapolation by chosing that sequence of basis states and the corresponding sequence of approximated eigenstates which minimizes the energy dependence on the energy variance and fitting a linear function to the last data points, see Figure 5.1.

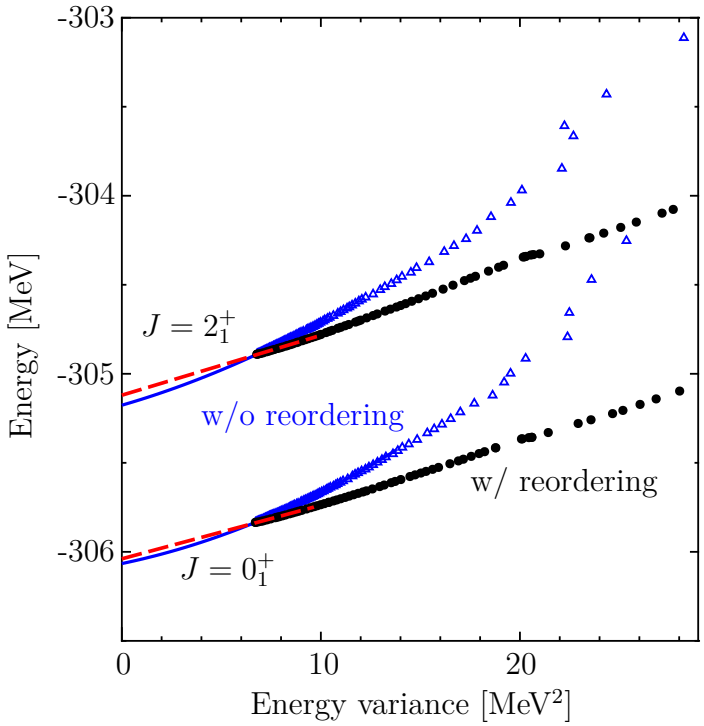

Figure 5.1.: Ground-state energy and the energy of the first excited state of a sequence of approximated eigenstates with (●) and without (△) reordering of the basis states versus their energy variance for ^{64}Ge. The sequence of approximated eigenstates has been computed in a MCSM calculation with subsequent SCG method using the PFG9B3 interaction [43, 44] and the $pfg_{9/2}$ shell as valence space. An extrapolation to vanishing energy variance has been done for both cases: A second-order polynomial has been fitted to the data points without reordering (solid blue line) and a linear function has been fitted to the reordered data points (dashed red line). Taken from [42].

Chapter 6

Applications and Benchmarks

We employ the importance-truncated shell model for the calculation of energies and spectroscopic observables of low-lying states of the nuclei ^{56}Ni and ^{64}Ge in the pf and $pfg_{9/2}$ shell, respectively. In Section 6.1, we demonstrate the robustness of the importance truncation by comparing results of ^{56}Ni computed in the IT-SM and the conventional shell model. In Section 6.2, we apply the IT-SM to ^{64}Ge, which is beyond the reach of the conventional shell model. This nucleus has been described using the same valence space and interaction in the MCSM and therefore offers a good opportunity to benchmark the IT-SM versus the MCSM.

6.1. IT-SM study of ^{56}Ni

As a first application of the IT-SM, we study low-lying energy levels of ^{56}Ni. We adopt the pf shell on top of a ^{40}Ca core as valence space. The corresponding full m-scheme dimension is 1.09×10^9, which is at the limit of a standard shell-model calculation. We remark that this model space contains only $0\hbar\omega$ harmonic-oscillator states and does not give rise to center-of-mass contaminations. The Hamilton matrix is constructed in the importance-truncated model space using the KB3 interaction [35]. We compare the results to conventional shell-model calculations carried out using the ANTOINE code [36]. Furthermore, we demonstrate that not only energies but also other observables can be calculated in the framework of the IT-SM. As a first test case, we compute electromagnetic observables for ^{56}Ni using the eigenstates obtained in an IT-SM calculation.

6.1.1. Excitation Spectrum

We start from a conventional shell-model calculation for ^{56}Ni in a $T_{\mathrm{max}} = 2$ truncated model space and construct the importance-truncated model spaces for a sequence of ten importance thresholds in the range of $\kappa_{\mathrm{min}} = 10^{-5}$ to 10^{-4}. For each κ_{min}, we diagonalize the Hamilton matrix computed in the respective importance-truncated model space and extrapolate the eigenenergies to vanishing importance threshold. In this way, we approximately account for basis states which are excluded from the importance-truncated model space because of their importance measure.

We furthermore reduce the computational effort of the IT-SM calculation by introducing a reference threshold C_{min} that restricts the size of the reference space used as input for each iteration. In Figure 6.1, we show a sequence of IT-SM calculations for the ground-state energy of ^{56}Ni for five reference thresholds C_{min} spanning one order of magnitude. We also show the dependence of the dimension of the importance-truncated model space on the importance threshold κ_{min} and the reference threshold C_{min}. As expected, for each reference threshold C_{min}, the energy eigenvalues approach the exact energy with decreasing κ_{min}. Moreover, for smaller values of the reference threshold, the κ_{min}-sequence of energy eigenvalues is lowered by some offset. This is due to the inclusion of more basis states in the reference space used as input for the next iteration. A larger reference space gives rise to a more extensive variety of possible basis states and hence larger importance-truncated model spaces, which are better suited for the precise description of the eigenstates. In order to quantify this statement, we consider an IT-SM calculation for $\kappa_{\mathrm{min}} = 10^{-5}$ and two different reference thresholds at the $T_{\mathrm{max}} = 6 \to T_{\mathrm{max}} = 8$ level: For $C_{\mathrm{min}} = 10^{-4}$, 1.4×10^6 basis states are selected from the $T_{\mathrm{max}} = 6$ importance-truncated model space to constitute the reference space for the iteration at the $T_{\mathrm{max}} = 8$ level, yielding 2.1×10^7 basis states. In contrast, if we use a reference threshold of $C_{\mathrm{min}} = 10^{-3}$, the corresponding reference space contains significantly less basis states, namely 5.5×10^4, from which we construct 6.8×10^6 basis states. Although the given set of reference thresholds is chosen to cover one order of magnitude, the extrapolated energies are in good agreement. Their maximum deviation is only 20 keV for the smallest and largest value of C_{min}. For the following discussion, we employ $C_{\mathrm{min}} = 10^{-4}$ as reference threshold because it provides the most precise results for the set of reference thresholds.

The energy eigenvalues of the six lowest eigenstates of ^{56}Ni obtained in an IT-SM calculation for $T_{\mathrm{max}} = 8$ are shown in Figure 6.2. As expected from the variational principle, they approach the exact energy monotonically from above for decreasing κ_{min}. We extrapolate to vanishing importance threshold by fitting a third-order polynomial to the energies and evaluating it for $\kappa_{\mathrm{min}} = 0$. The error bands representing the

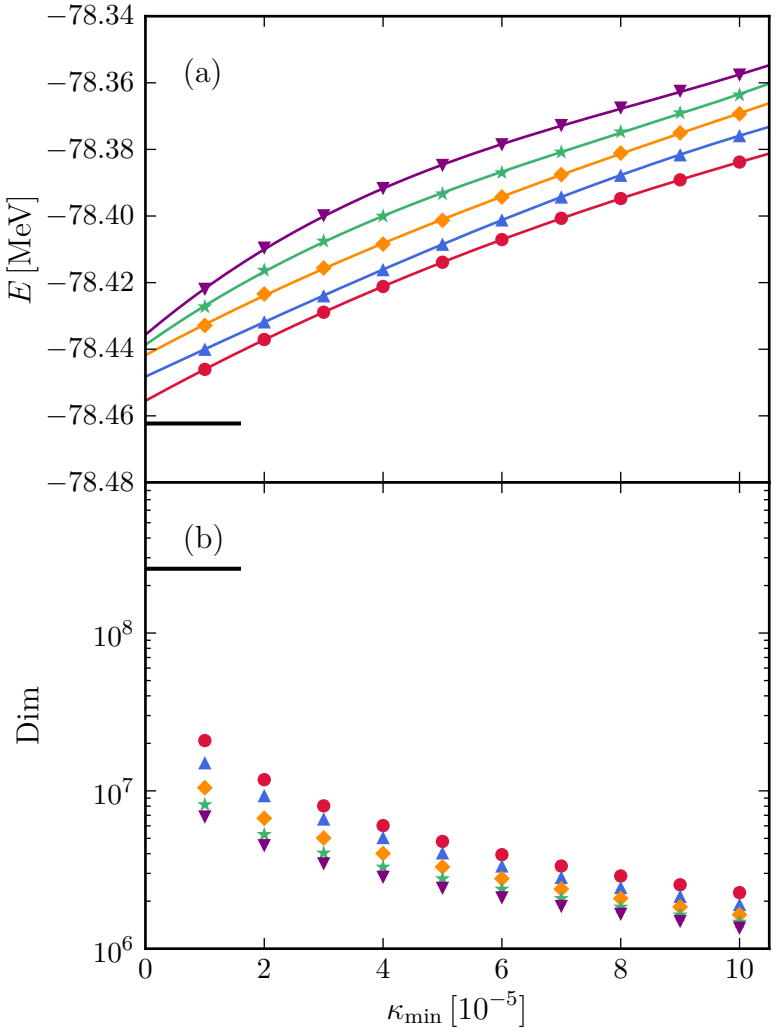

Figure 6.1.: (a) Threshold dependence and extrapolation of the ground-state energy of ^{56}Ni obtained in a sequence of IT-SM calculations for $T_{\max} = 8$ and $C_{\min} = \{10^{-4}$ (●), $2.5 \cdot 10^{-4}$ (▲), $5 \cdot 10^{-4}$ (◆), $7.5 \cdot 10^{-4}$ (★), 10^{-3} (▼)$\}$ using the KB3 interaction. The black line indicates the exact eigenvalue computed with the ANTOINE code [36] for the same $T_{\max}$ and interaction. In panel (b), the corresponding importance-truncated and m-scheme model-space dimensions are shown.

uncertainty of the extrapolations are shown, but hardly visible on this scale. For the ground-state energy, e.g., the uncertainty is less than 1 keV. The extrapolated energies are good approximations to the exact energies, e.g. the ground-state energy deviates from the exact value by only some keV and the maximum deviation of the considered eigenstates from the exact values is a few tens of keV for the first excited state, see Table 6.1. As illustrated in Figure 6.1 and mentioned above, a lowering of the reference threshold $C_{\min}$ yields a lowering of the corresponding $\kappa_{\min}$-sequence of energies and consequently of the threshold-extrapolated results. We therefore expect to improve the agreement of the extrapolated and exact energies by choosing smaller values of $C_{\min}$.

In order to probe the quality of the simple threshold extrapolation, we carry out the extrapolation again using the constrained threshold-extrapolation technique. We define a set of energy functions $\tilde{E}_\lambda(\kappa_{\min})$ for five values of $\lambda = \{0, 0.5, 1, 1.5, 2\}$, where the eigenenergies and the perturbatively corrected energies are recovered for $\lambda = 0$ and $\lambda = 1$, respectively. We fit third-order polynomials simultaneously to this set of energy functions $\tilde{E}_\lambda(\kappa_{\min})$ under the constraint that the extrapolated values are identical for $\kappa_{\min} = 0$. The constrained threshold extrapolation of the six lowest eigenstates of ^{56}Ni is shown in Figure 6.3. Again, the extrapolated energies are in good agreement with the exact energies and the deviations from the exact values are of the same order as in the case of the simple extrapolation technique, see Table 6.1. We have introduced the constrained threshold-extrapolation technique in order to stabilize the extrapolation, but since both methods provide accurate results, we do not favor neither of the techniques. In the following, we use the simple extrapolation technique for the evaluation of the IT-SM results because this allows us to treat energies and observables on the same footing. There is no analog procedure to the constrained

J^+	E_{ANT} [MeV]	E_{s} [MeV]	E_{c} [MeV]
0_1^+	-78.462	$-78.456(0)$	$-78.452(2)$
2_1^+	-73.292	$-73.247(6)$	$-73.234(10)$
4_1^+	-72.472	$-72.444(4)$	$-72.432(8)$
3_1^+	-71.967	$-71.940(4)$	$-71.928(8)$
6_1^+	-71.433	$-71.417(3)$	$-71.408(5)$
5_1^+	-71.272	$-71.249(4)$	$-71.238(7)$

Table 6.1.: Energies of the six lowest eigenstates of ^{56}Ni obtained in IT-SM calculations for $T_{\max} = 8$ and $C_{\min} = 10^{-4}$ with subsequent simple and constrained threshold extrapolation, E_{s} and E_{c}, respectively. The extrapolation uncertainties are given. For comparison, the exact energies E_{ANT} computed with the ANTOINE code are shown.

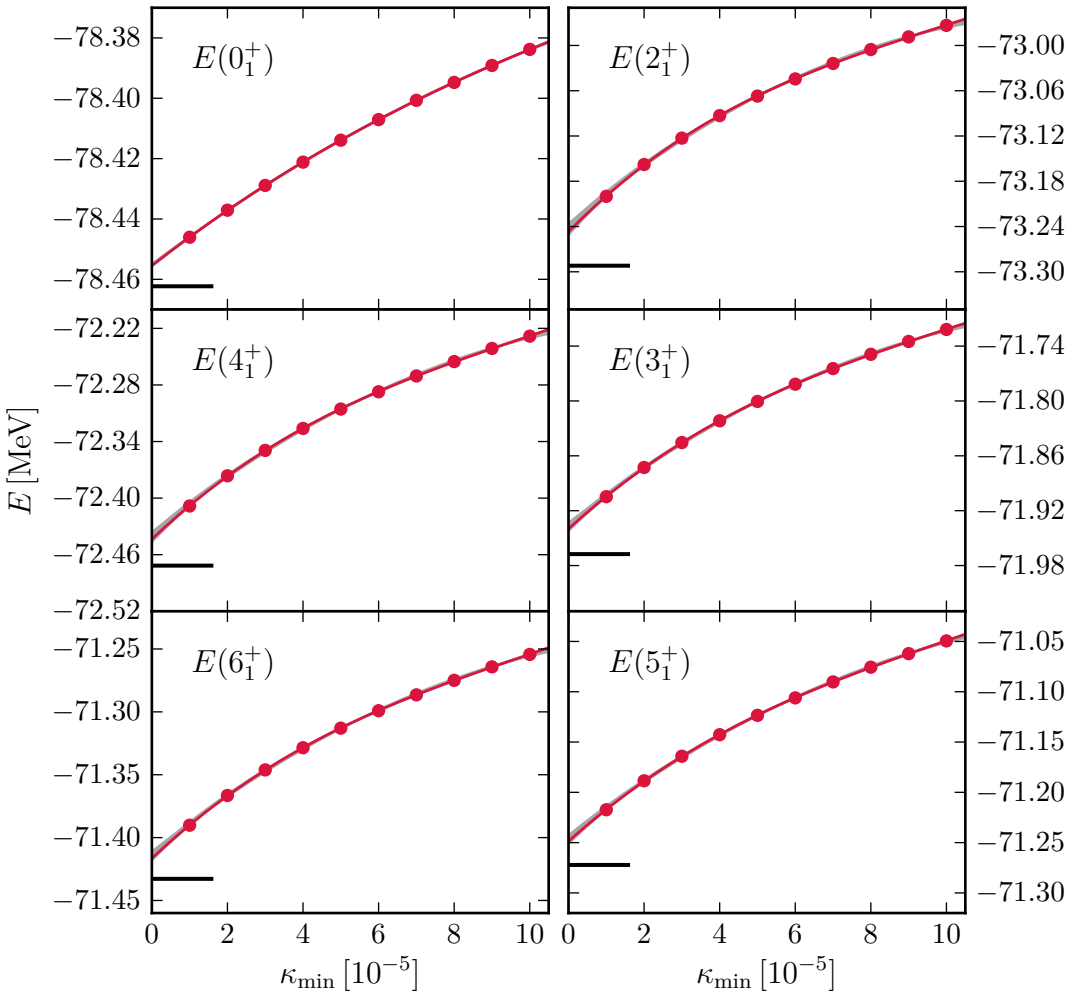

Figure 6.2.: Threshold extrapolation of the six lowest eigenstates of ^{56}Ni obtained in IT-SM calculations for $T_{\max} = 8$ and $C_{\min} = 10^{-4}$ using the KB3 interaction. The red lines show the fit of a third-order polynomial to the energies $E(\kappa_{\min})$, the grey error bands indicate the uncertainty of the fit. The black horizontal lines show the exact eigenvalues computed with the ANTOINE code [36] for the same $T_{\max}$ and interaction.

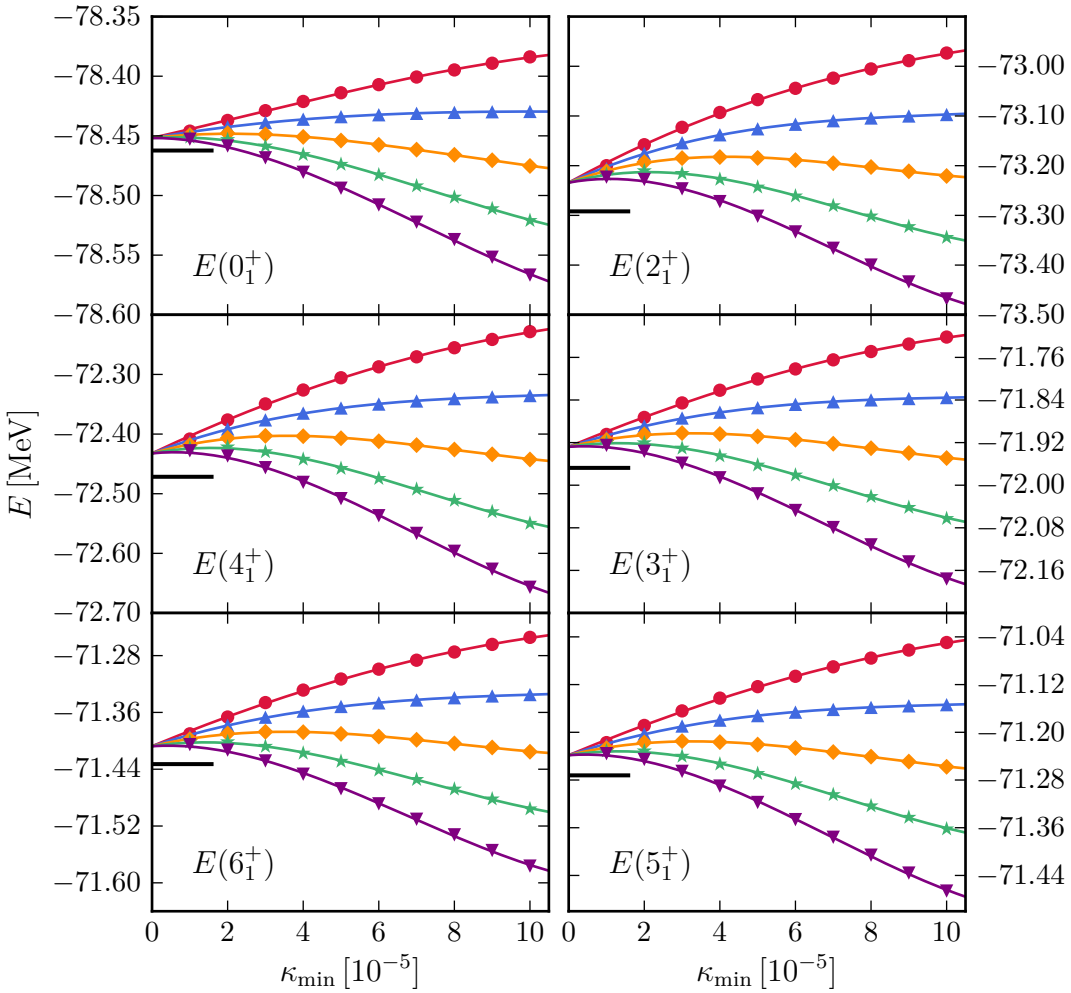

Figure 6.3.: Threshold extrapolation of the six lowest eigenstates of ^{56}Ni obtained in IT-SM calculations for $T_{\max} = 8$ and $C_{\min} = 10^{-4}$ using the KB3 interaction. The energy functions $\tilde{E}_\lambda(\kappa_{\min})$ are shown for the parameter set $\lambda = \{0\ (\bullet),\ 0.5\ (\blacktriangle),\ 1\ (\blacklozenge),\ 1.5\ (\bigstar),\ 2\ (\blacktriangledown)\}$. For $\lambda = 0$, the original energy $E(\kappa_{\min})$ is recovered, for $\lambda = 1$, we obtain the perturbatively corrected energy $E(\kappa_{\min}) + \Delta_{\text{excl}}$. The colored lines show the constrained fit for all data sets using third-order polynomials. The black lines indicate the exact eigenvalues computed with the ANTOINE code [36] for the same $T_{\max}$ and interaction.

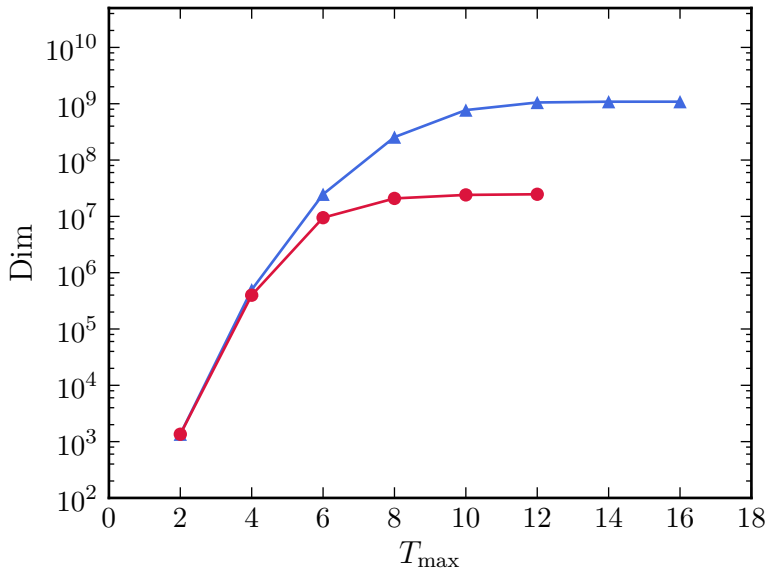

Figure 6.4.: Model-space dimension of ^{56}Ni in the conventional (▲) and importance-truncated (●) shell model ($\kappa_{\min} = 10^{-5}$, $C_{\min} = 10^{-4}$) as a function of the truncation $T_{\max}$. The importance-truncated model space has been set up for the simultaneous description of the six lowest eigenstates.

threshold extrapolation for the treatment of observables.

We demonstrate the computational superiority of the IT-SM over the conventional shell model by comparing the dimensions of the corresponding model spaces for several values of $T_{\max}$, see Figure 6.4. The dimension of the full model space is 1.09×10^9. As already mentioned, such dimensions are difficult to handle and are at the upper limit of standard shell-model calculations. For the IT-SM, we use the model space constructed for an importance threshold of $\kappa_{\min} = 10^{-5}$. The corresponding model-space dimension increases to a smaller extent with increasing $T_{\max}$ than in the conventional shell model and approximate saturation of the model-space size is already reached for $T_{\max} = 8$. In the conventional shell model, saturation does not start before $T_{\max} = 10$. For this $T_{\max}$, the IT-SM dimension is reduced by about two orders of magnitude compared to the conventional shell-model dimension. Note that the importance-truncated model spaces discussed above are constructed for the simultaneous description of six eigenstates. If we were only interested in the ground state, we would reduce the dimensions even further, gaining approximately one extra order of magnitude. Thus, the importance-truncation scheme allows an efficient reduction of the model-space dimensions and consequently of the computational effort for the computation and diagonalization of the Hamilton matrix. We have to keep in mind, however, that the computationally demanding part of an IT-SM calculation is the construction of the importance-truncated valence space.

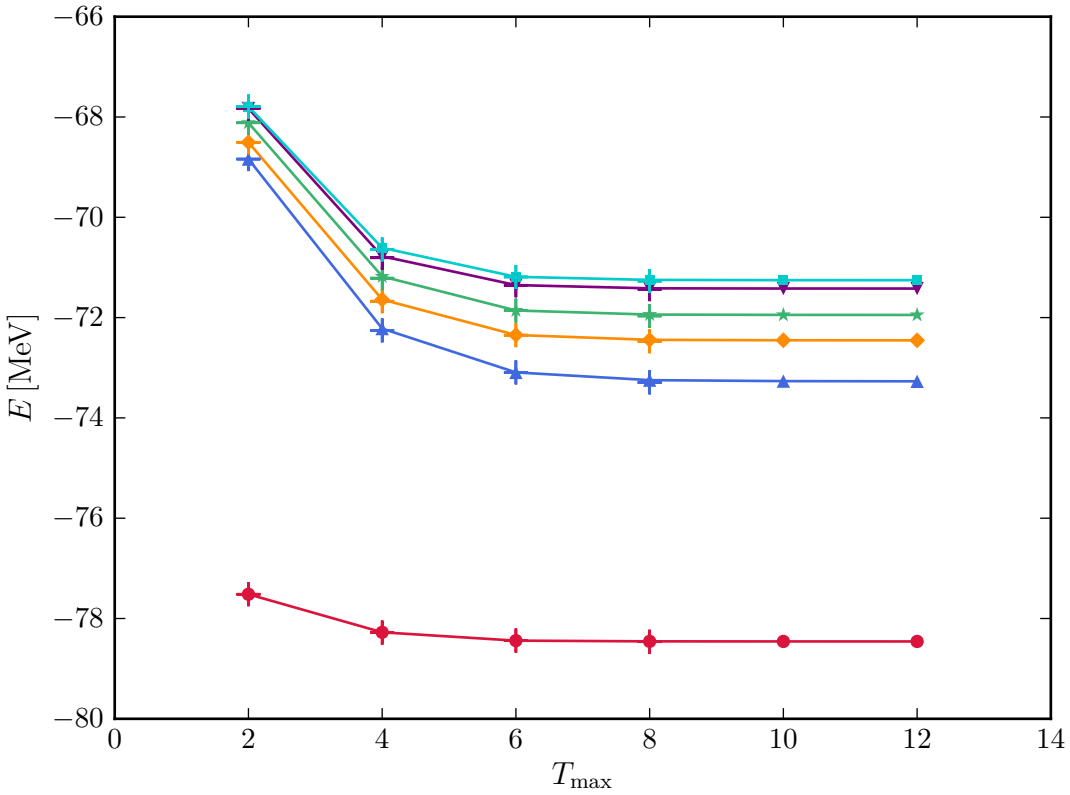

Figure 6.5.: Energies of the ground state and the five lowest excited states of ^{56}Ni as a function of the truncation parameter $T_{\max}$: $E(0_1^+)$ (●), $E(2_1^+)$ (▲), $E(4_1^+)$ (◆), $E(3_1^+)$ (★), $E(6_1^+)$ (▼), $E(5_1^+)$ (■). The crosses + denote the exact energies.

In Figure 6.5, the energies of the ground state and the first lowest excited states are shown as a function of $T_{\max}$. They are in excellent agreement with the exact energies, which are shown for $T_{\max} = 2, 4, 6$ and 8. This demonstrates the efficiency of the importance measure and the reliability of the threshold extrapolation.

The excitation spectrum of ^{56}Ni computed in IT-SM calculations and conventional shell-model calculations is shown in Figure 6.6. The spectra are in excellent agreement and small deviations are only visible for $T_{\max} = 4$, where the excitation energies computed in the IT-SM are about 30 keV higher than the exact excitation energies. This is due to the necessity of a proper coupling of basis states with up to 4p4h excitations, which is established only in another iteration via the reassessment of the previously constructed basis states. Furthermore, the threshold extrapolation typically works better for larger $T_{\max}$ spaces. In the NCSM and the IT-NCSM, we expect the relative energies to converge faster than the absolute energies. We do not observe this behavior in the IT-SM calculation for ^{56}Ni: In the iteration $T_{\max} = 6 \to T_{\max} = 8$, e.g., the absolute energy of the first excited state is lowered by 150 keV. The energy relative to the

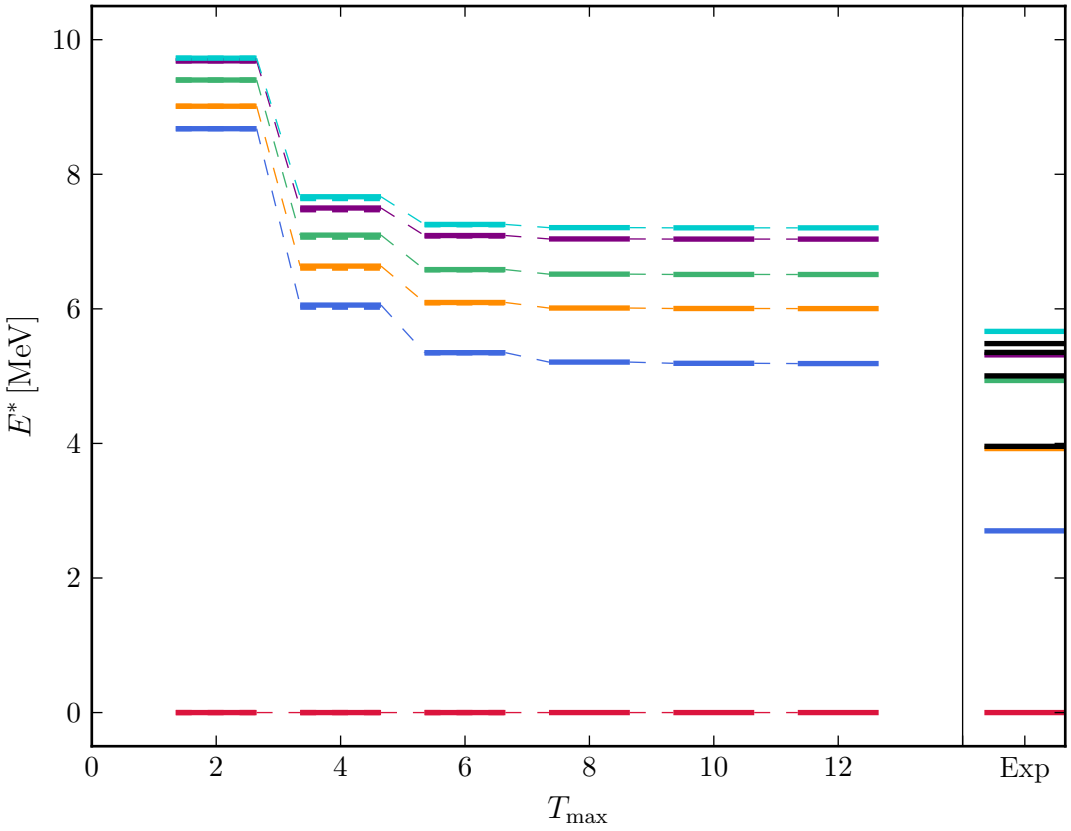

Figure 6.6.: Excitation spectrum of ^{56}Ni computed in IT-SM calculations for different $T_{\max}$ using the KB3 interaction. The solid lines denote the excitation energies of the states with $J^\pi = \{0_1^+, 2_1^+, 4_1^+, 3_1^+, 6_1^+, 5_1^+\}$. The excitation energies obtained in conventional shell-model calculations are plotted as dashed lines in the corresponding colors for $T_{\max} = 2$ to $T_{\max} = 8$. In the right column, the experimental spectrum [45] is shown. The computed energies are compared to the experimental ones by identifying the states via their J^π quantum numbers.

ground state is lowered by 140 keV. In the next iteration, the lowering of the energies is 20 keV in both cases. Finally, we remark that the excitation energies computed in the IT-SM do not reproduce the experimental spectrum shown in the right column of Figure 6.6. This is because the KB3 interaction is constructed for the description of nuclei with a few valence nucleons on top of the ^{40}Ca core. Shell-model calculations for nuclei in the mass region around ^{56}Ni using this interaction are rather poor [46].

6.1.2. Electromagnetic Observables

Electromagnetic observables such as multipole moments and transition strengths are an efficient probe for the structure of eigenstates, and are a test for the quality of a model. We give a short outline of this topic and refer the reader to [47] and standard textbooks for more details. Then, we show some electromagnetic observables of ^{56}Ni obtained in the IT-SM: We compute the electric quadrupole moment of the first excited state and the transition strengths of an electric and a magnetic transition, respectively. Since the eigenstates are computed using the KB3 interaction, we do not expect the results to agree well with the experimental data. Therefore, we restrict ourselves to comparing the results to conventional shell-model calculations in order to demonstrate the validity of the IT-SM.

Electromagnetic transitions are mediated by the interaction of an external electromagnetic field with the nucleus. The electromagnetic field can be expanded in multipoles. The particular components are characterized by their multipolarity λ and corresponding substates μ. An electromagnetic transition is mediated by one of these components and can be of electric ($\sigma = \mathrm{E}$) or magnetic ($\sigma = \mathrm{M}$) character. The transition probability of an initial state i to a final state f is given by Fermi's "golden rule":

$$T_{fi}^{(\sigma\lambda\mu)} = \frac{2}{\epsilon_0 \hbar} \frac{\lambda+1}{\lambda[(2\lambda+1)!!]^2} \left(\frac{E_\gamma}{\hbar c}\right)^{2\lambda+1} \left|\langle \xi_f J_f M_f | \mathbf{T}_{\sigma\lambda\mu} | \xi_i J_i M_i \rangle\right|^2 . \tag{6.1}$$

The transition energy is denoted by E_γ and $\mathbf{T}_{\sigma\lambda\mu}$ is the operator associated with the multipole radiation field $\sigma\lambda\mu$. The initial and the final state are characterized by ξ_i and ξ_f, respectively, which carry all other quantum numbers than the angular momentum J and its z-projection M. Since the magnetic substates are normally not observed separately, we average over the possible initial substates and sum over all final substates. Then, we obtain

$$T_{fi}^{(\sigma\lambda)} = \frac{1}{2J_i+1} \sum_{M_i,\mu,M_f} T_{fi}^{(\sigma\lambda\mu)} \tag{6.2}$$

$$= \frac{2}{\epsilon_0 \hbar} \frac{\lambda+1}{\lambda[(2\lambda+1)!!]^2} \left(\frac{E_\gamma}{\hbar c}\right)^{2\lambda+1} B(\sigma\lambda : \xi_i J_i \to \xi_f J_f) \tag{6.3}$$

for the transition probability. The prefactor is related to the density of states. All physics is absorbed in the reduced transition probability, also termed transition strength

$$B(\sigma\lambda : \xi_i J_i \to \xi_f J_f) = \frac{1}{2J_i+1} \left|(\xi_f J_f || \boldsymbol{T}_{\sigma\lambda} || \xi_i J_i)\right|^2 . \tag{6.4}$$

The components of the operator $\boldsymbol{T}_{\sigma\lambda}$ for electric and magnetic transitions are given by

$$\mathbf{Q}_{\lambda\mu} = \zeta \sum_{j=1}^{A} e_j \mathbf{r}_j^{\lambda} Y_{\lambda\mu}(\boldsymbol{\Omega}_j), \tag{6.5}$$

$$\mathbf{M}_{\lambda\mu} = \zeta \frac{\mu_N}{\hbar c} \sum_{j=1}^{A} \left(\frac{2}{\lambda+1} g_j^l \vec{\boldsymbol{l}}_j + g_j^s \vec{\boldsymbol{s}}_j \right) \cdot \boldsymbol{\nabla} \left(\mathbf{r}_j^{\lambda} Y_{\lambda\mu}(\boldsymbol{\Omega}_j) \right), \tag{6.6}$$

respectively. We choose the phase factors $\zeta = 1$ according to the Condon-Shortley phase convention [47]. Here, $Y_{\lambda\mu}(\Omega)$ denotes the spherical harmonics and e_j is the electric charge of the nucleon j. The orbital angular momentum and the spin of the nucleons are referred to by $\vec{\boldsymbol{l}}$ and $\vec{\boldsymbol{s}}$, and g^l and g^s are the respective gyromagnetic ratios. The quantity μ_N denotes the nuclear magneton. We use the bare values for the electric charge and the gyromagnetic ratios, but effective values can be chosen which approximately account for core effects [47]. The reduced matrix element $(\xi_f J_f || \boldsymbol{T}_{\sigma\lambda} || \xi_i J_i)$ in (6.4) can be simplified via an expansion in terms of reduced single-particle matrix elements, see e.g. Equations (6.22) to (6.24) in [47].

The static electric and magnetic multipole moment of a nucleus in a given state is defined as the expectation value of the corresponding multipole operator in the $\mu = 0$ component evaluated in the state with maximum angular-momentum projection M.

$$\mathcal{M}_{\sigma\lambda}(J^{\pi}) = \langle \xi JM = J | \mathbf{T}_{\sigma\lambda 0} | \xi JM = J \rangle . \tag{6.7}$$

The conventional magnetic dipole moment μ and electric quadrupole moment Q, e.g., are given by:

$$\frac{1}{c}\mu = \frac{4\pi}{3} \frac{J}{(J+1)(2J+1)} (\xi J || \mathbf{M}_{10} || \xi J) , \tag{6.8}$$

$$eQ = \frac{16\pi}{5} \frac{J(2J-1)}{(J+1)(2J+1)(2J+3)} (\xi J || \mathbf{Q}_{20} || \xi J) . \tag{6.9}$$

As a first example, we consider the quadrupole moment of the first excited state of ^{56}Ni: We use the wave functions obtained in IT-SM calculations for a sequence of importance thresholds $\kappa_{\min}$ for the computation of the quadrupole moment $Q(\kappa_{\min})$ according to (6.9) and extrapolate to vanishing importance threshold using the simple extrapolation technique. In Figure 6.7 (a), we show $\kappa_{\min}$-sequences of the quadrupole moment $Q(\kappa_{\min})$ for the reference thresholds $C_{\min} = 10^{-4}$ and $C_{\min} = 2.5 \times 10^{-4}$. For decreasing $\kappa_{\min}$, the quadrupole moment approaches the exact value. Moreover, the smaller reference threshold provides a better approximation to the quadrupole moment obtained in the conventional shell-model calculation. The threshold extrapolation overestimates the exact value for both reference thresholds. Here, the IT-SM for the

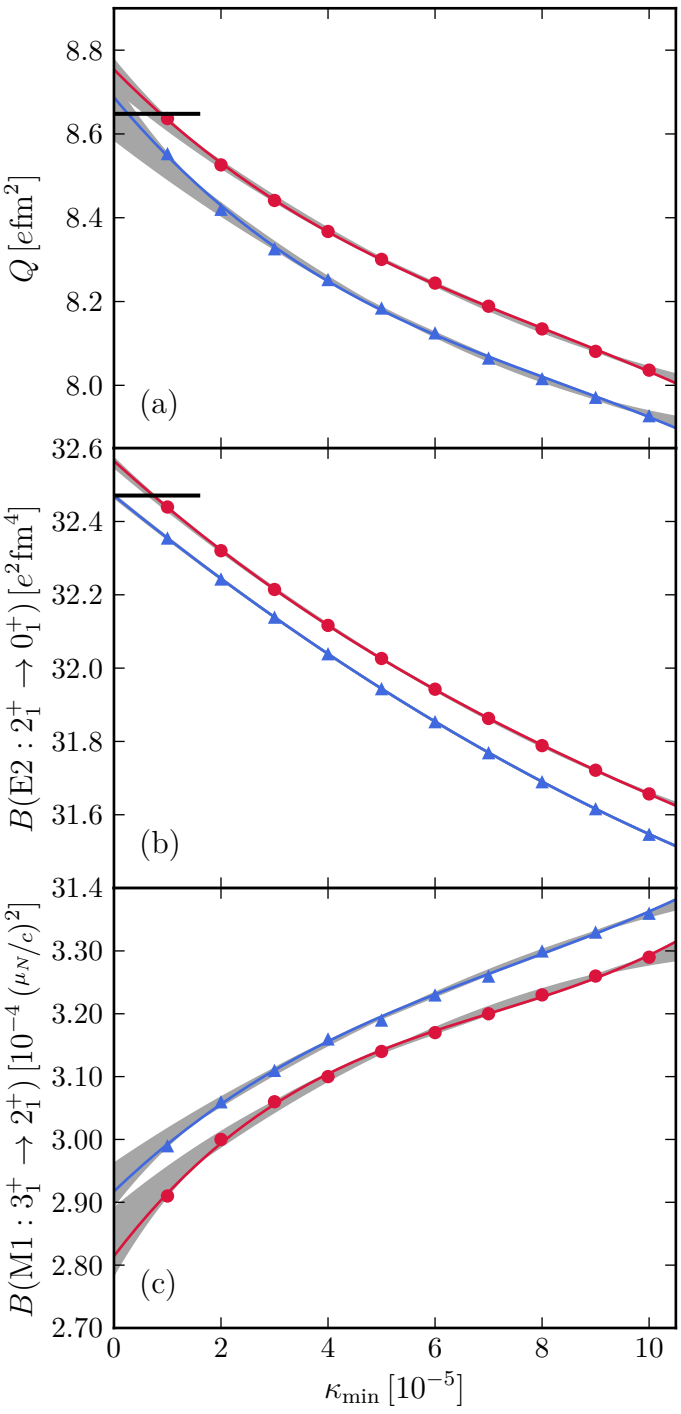

Figure 6.7.: Threshold extrapolations of electromagnetic observables of ^{56}Ni computed in the IT-SM for $T_{\max} = 8$ and the reference thresholds $C_{\min} = 10^{-4}$ (●) and $C_{\min} = 2.5 \times 10^{-4}$ (▲). Panel (a) illustrates the quadrupole moment of the first excited state (2_1^+). In panel (b) and (c), the threshold extrapolations of the reduced transition probabilities $B(\mathrm{E2}: 2_1^+ \to 0_1^+)$ and $B(\mathrm{M1}: 2_1^+ \to 3_1^+)$ are shown. The exact values are indicated by the horizontal black lines in (a) and (b).

smallest combination of importance and reference thresholds without extrapolation to $\kappa_{\min} \to 0$ provides the best result. Its deviation from the exact value is less than 0.01 $e\text{fm}^2$. One can conclude that the importance-truncated model space already contains all basis states necessary for the description of the quadrupole moment for this set of thresholds.

We observe a similar behavior for the IT-SM results for the reduced transition probabilities $B(\text{E2} : 2_1^+ \to 0_1^+)$ and $B(\text{M1} : 2_1^+ \to 3_1^+)$ shown in Figure 6.7 (b) and (c), respectively. For decreasing $\kappa_{\min}$, the transition strengths approach a fix value, which, considering the combination of smallest thresholds, agrees very well with the exact value for the electric transition strength (Figure 6.7 (b)). For the magnetic transition, we abstain from the comparison to the exact value because the ANTOINE output files only show four digits after the decimal point. Although the extrapolated results exceed the exact values, they are still in good agreement.

In Figure 6.8, we show the extrapolated IT-SM results for the quadrupole moment and the reduced transition probabilities as functions of the truncation $T_{\max}$. For the quadrupole moment and the electric transition strength, the IT-SM results consistently overestimate the exact values. This is due to the threshold extrapolation, which misses the exact results. Thus, the threshold extrapolation for the larger $C_{\min}$ approximates the exact values better although their IT-SM model spaces are smaller and less suited to accurately describe nuclear eigenstates. To the precision given by ANTOINE, the IT-SM results for the magnetic transition strength are compatible with the exact ones, for which the possible range of values is indicated by the error bars.

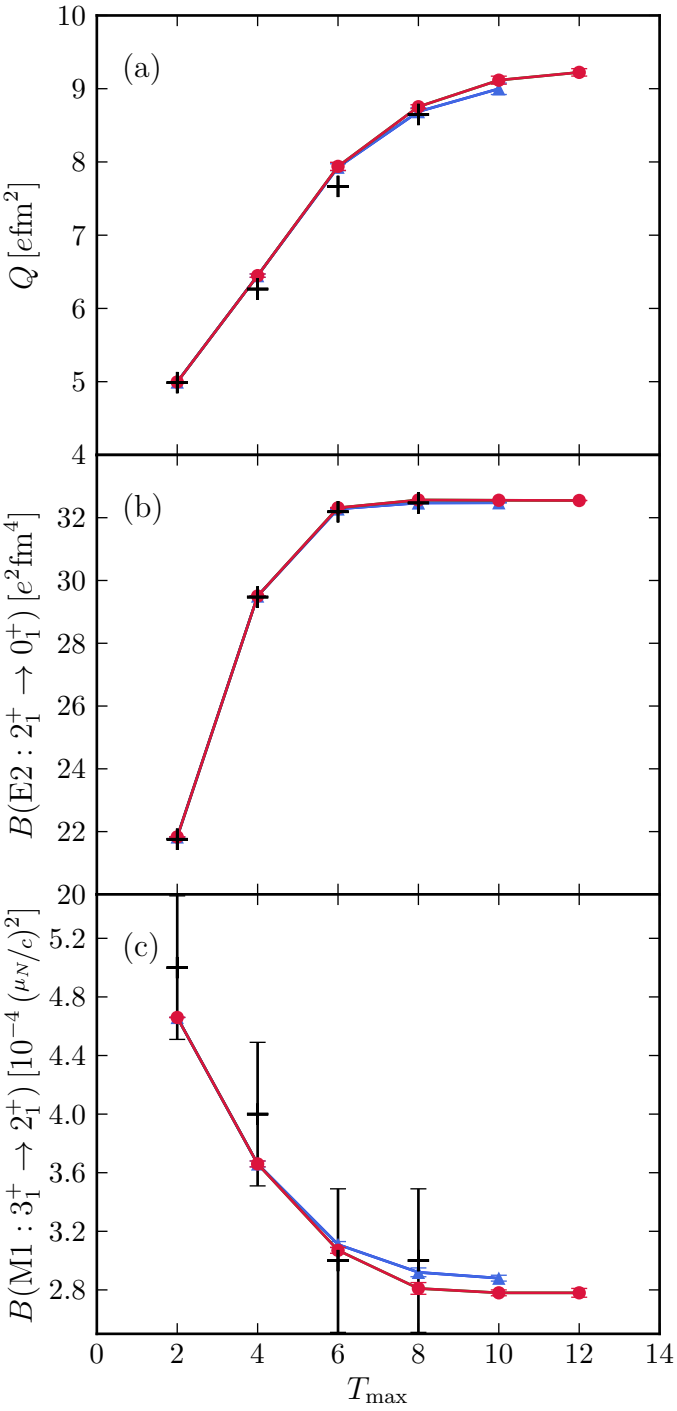

Figure 6.8.: Quadrupole moment of the 2_1^+ state (a) and the reduced transition probabilities $B(\mathrm{E2}: 2_1^+ \to 0_1^+)$ (b) and $B(\mathrm{M1}: 2_1^+ \to 3_1^+)$ (c) of ^{56}Ni as functions of $T_{\max}$. The electromagnetic observables are computed in IT-SM calculations for the reference thresholds $C_{\min} = 10^{-4}$ (●) and $C_{\min} = 2.5 \times 10^{-4}$ (▲). The exact values are indicated (+). Due to the insufficient number of digits in the ANTOINE output files for the magnetic transition strength, error bars are shown which illustrate the uncertainties due to rounding (c). In all plots, the uncertainties of the threshold extrapolations are indicated by error bars.

6.2. IT-SM study of ^{64}Ge

In order to demonstrate that the importance truncation allows an extension of the shell model to nuclei and model spaces beyond the reach of the conventional shell model, we consider ^{64}Ge in the $pfg_{9/2}$ shell. The corresponding m-scheme dimension of the full model space is 1.7×10^{14}. So far, we have carried out IT-SM calculations up to $T_{\max} = 8$ and $T_{\max} = 10$ for different reference thresholds. These truncated model spaces are already intractable for conventional shell-model calculations, their m-scheme dimensions are 1.5×10^{11} and 3.5×10^{12}, respectively.

By employing the $pfg_{9/2}$ shell as valence space, the valence nucleons are allowed to be excited by up to $1\hbar\omega$. Thus, the model space contains basis states with coupled intrinsic and center-of-mass components giving rise to spurious states. We apply the approximate procedure described in Chapter 3 in order to deal with these spurious states and use the Hamiltonian

$$\mathbf{H} = \mathbf{H}_{\text{nuc}} + \beta \mathbf{H}_{\text{cm}} \tag{6.10}$$

for the solution of the eigenvalue problem. We obtain the matrix elements of the nuclear Hamiltonian from the effective interaction PFG9B3 [43, 44] and use Equation (3.15) to calculate the matrix elements of the center-of-mass Hamiltonian. In the following, we choose $\beta = 1$ as suggested in [32] unless otherwise specified.

We employ the eigenstates obtained in a conventional shell-model calculation with $T_{\max} = 4$ as starting point for the iterative construction of the importance-truncated model space. This model space is always constructed for the simultaneous description of the six lowest eigenstates. As for ^{56}Ni, we carry out IT-SM calculations for a sequence of importance thresholds and extrapolate to $\kappa_{\min} \to 0$ in order to account for excluded configurations.

In Figure 6.9, we show the simple and the constrained threshold extrapolation for the three lowest energy levels of ^{64}Ge for $T_{\max} = 8$. We use third- and fifth-order polynomials for the simple threshold extrapolation, and third-order polynomials for the constrained threshold extrapolation. The results obtained using the two extrapolation techniques are in reasonable agreement, e.g. they differ by approximately ten keV for the ground-state energy obtained for the third-order polynomial fits. The constrained threshold extrapolation artificially raises the extrapolated energies. Since the extrapolation corresponding to the fit of the fifth-order polynomial allows for a stronger bending, it provides the best results. In the following, we therefore use the extrapolated energies obtained in the simple threshold extrapolation using fifth-order polynomials for the fits.

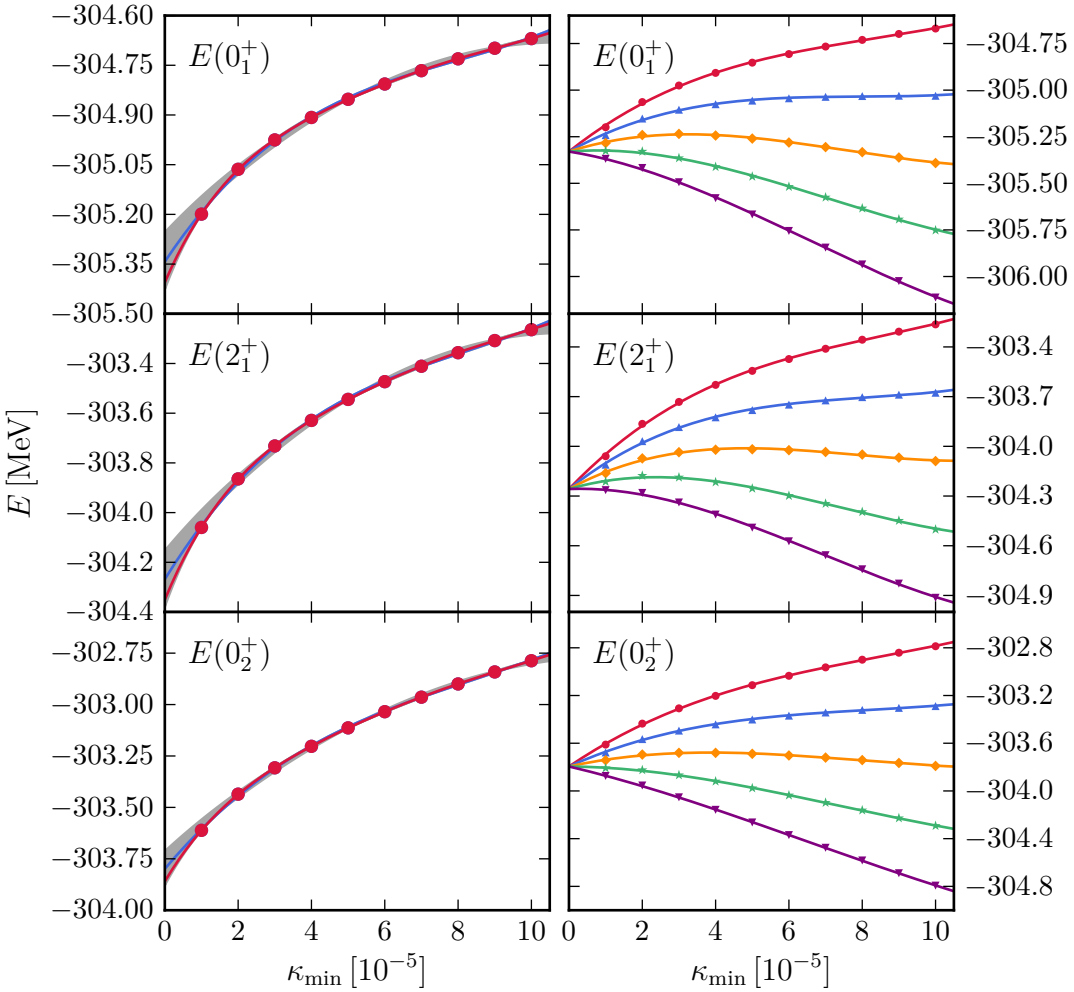

Figure 6.9.: Threshold extrapolation of the energy eigenvalues of the three lowest eigenstates of ^{64}Ge. The energies $E(\kappa_{\min})$ are computed in IT-SM calculations for $T_{\max} = 8$ using the PFG9B3 interaction and the reference threshold $C_{\min} = 2 \times 10^{-4}$. In the left column, the simple threshold-extrapolation technique is applied to the energy eigenvalues $E(\kappa_{\min})$ using third-order (blue line) and fifth-order polynomials (red line) for the fit. In the right column, the constrained threshold-extrapolation technique is applied to the energy functions $\tilde{E}_\lambda(\kappa_{\min})$ for $\lambda = \{0\ (\bullet), 1\ (\blacktriangle), 2\ (\blacklozenge), 3\ (\bigstar), 4\ (\blacktriangledown)\}$, respectively. The data points are fitted to third-order polynomials.

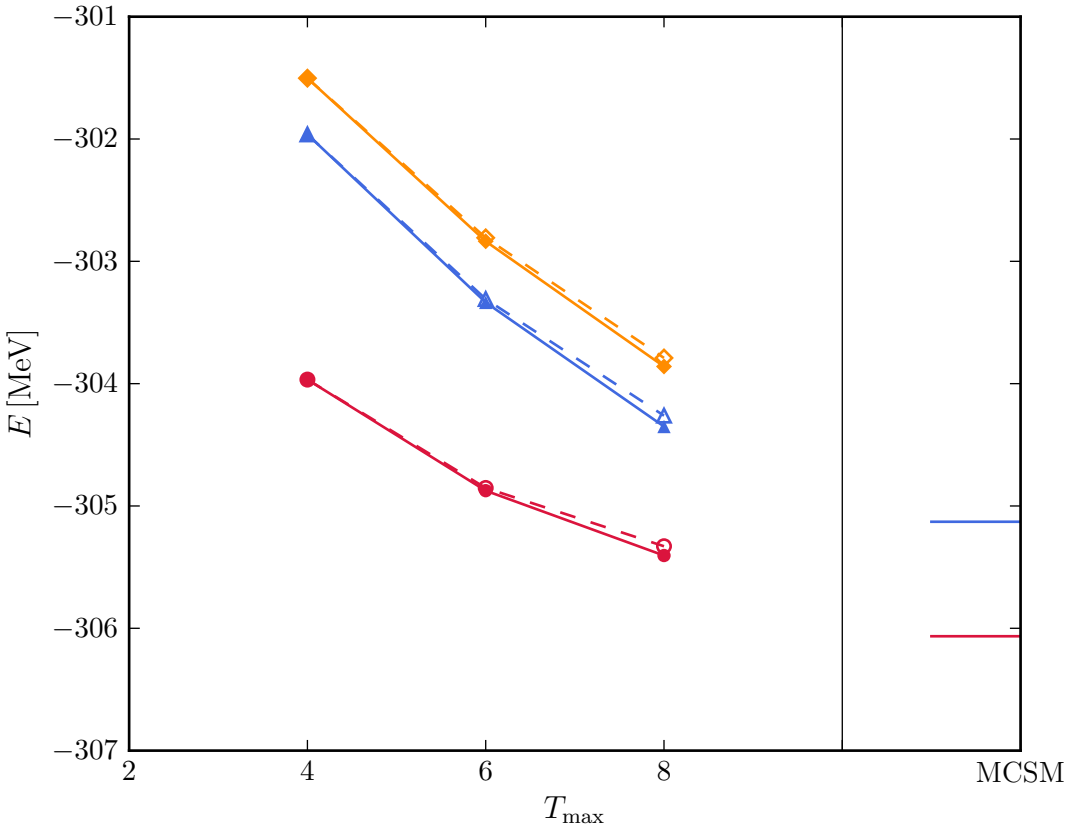

Figure 6.10.: IT-SM energies of the three lowest eigenstates of ^{64}Ge using the reference thresholds $C_{\mathrm{min}} = 2 \times 10^{-4}$ (filled symbols) and $C_{\mathrm{min}} = 5 \times 10^{-4}$ (open symbols) as a function of T_{max}. The filled and open symbols are connected via continuous and dashed lines, respectively. Note that the second excited state changes parity for different T_{max}, see Figure 6.11.

In Figure 6.10, we show the energies obtained in IT-SM calculations as a function of T_{max} and compare the results to a MCSM calculation with subsequent energy-variance extrapolation (Chapter 5, [42]). For increasing T_{max}, basis states with higher numbers of particle-hole excitations are included in the importance-truncated model space, making it better suited for the description of the particular eigenstates. This becomes manifest in a lowering of the energy eigenvalues. Figure 6.10 also illustrates the dependence of the IT-SM energies on the reference threshold: The energies corresponding to the smaller reference threshold $C_{\mathrm{min}} = 2 \times 10^{-4}$ are lower than the IT-SM results obtained for $C_{\mathrm{min}} = 5 \times 10^{-4}$. The effect is moderate; for the three states considered here, the energies are lowered by less than 100 keV for $T_{\mathrm{max}} = 8$. Since the offset in the energies caused by the different reference thresholds is approximately constant, we expect the excitation spectra to be independent of C_{min}. The energy eigenvalues shown in Figure 6.10 are clearly not yet converged and are above the MCSM values by several hundreds

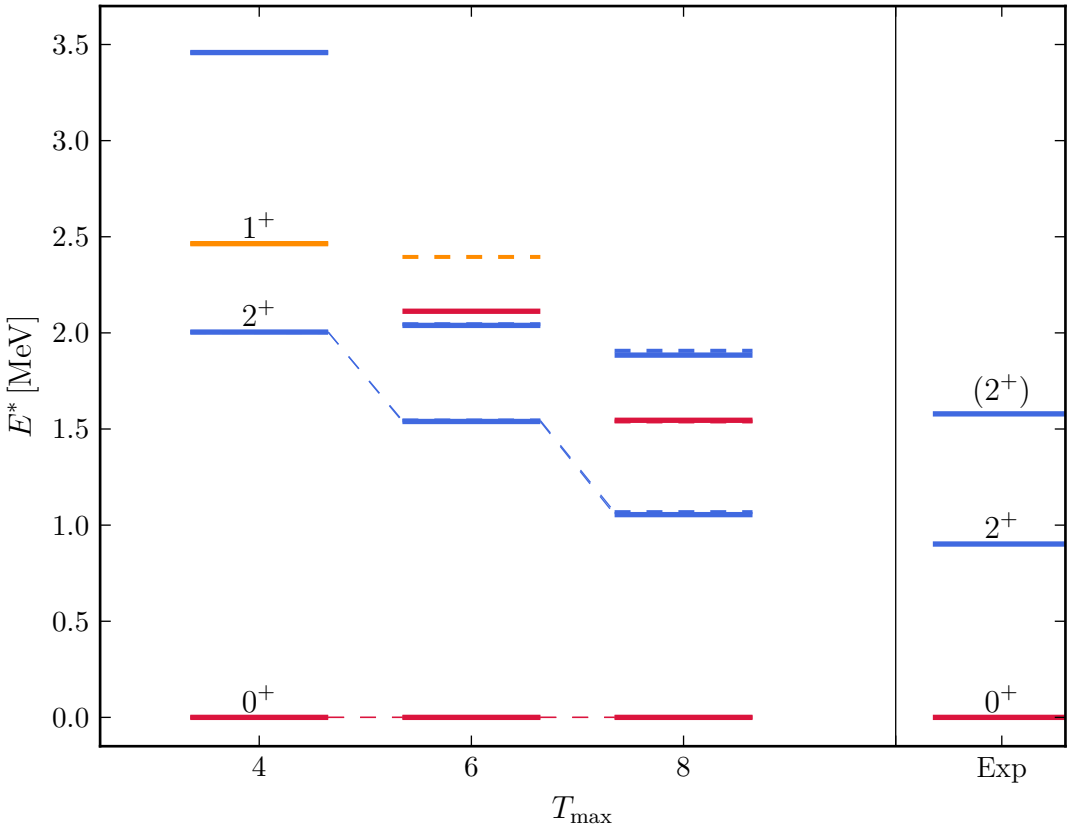

Figure 6.11.: Lowest part of the excitation spectrum of ^{64}Ge obtained in IT-SM calculations for the reference thresholds $C_{\min} = 2 \times 10^{-4}$ (solid lines) and $C_{\min} = 5 \times 10^{-4}$ (dashed lines). States with different J^π quantum numbers are plotted in different colors. The corresponding experimental spectrum is shown in the right column [48].

of keV.

We show the lowest part of the excitation spectrum of ^{64}Ge in Figure 6.11. As expected from the above discussion, the three lowest eigenstates agree well for the two reference thresholds considered. For the third excited state, on the contrary, the excitation energies differ by about 300 keV for $T_{\max} = 6$ and the J^π quantum numbers are not identical. This is not so much an effect of $C_{\min}$ but is rather due to a strong mixing of the almost degenerate eigenstates in this energy region. Although the excitation energies are not yet fully converged, they are in good agreement with the experimental data already for $T_{\max} = 8$, e.g. we obtain an excitation energy of 1.07 MeV for the 2_1^+ state. The experimental value is 0.90 MeV [48]. We expect further improvement for higher $T_{\max}$. Note that the J^π quantum numbers of the excited states can change in the course of the iteration. This is due to the rapid increase of basis states contained in the importance-truncated model space.

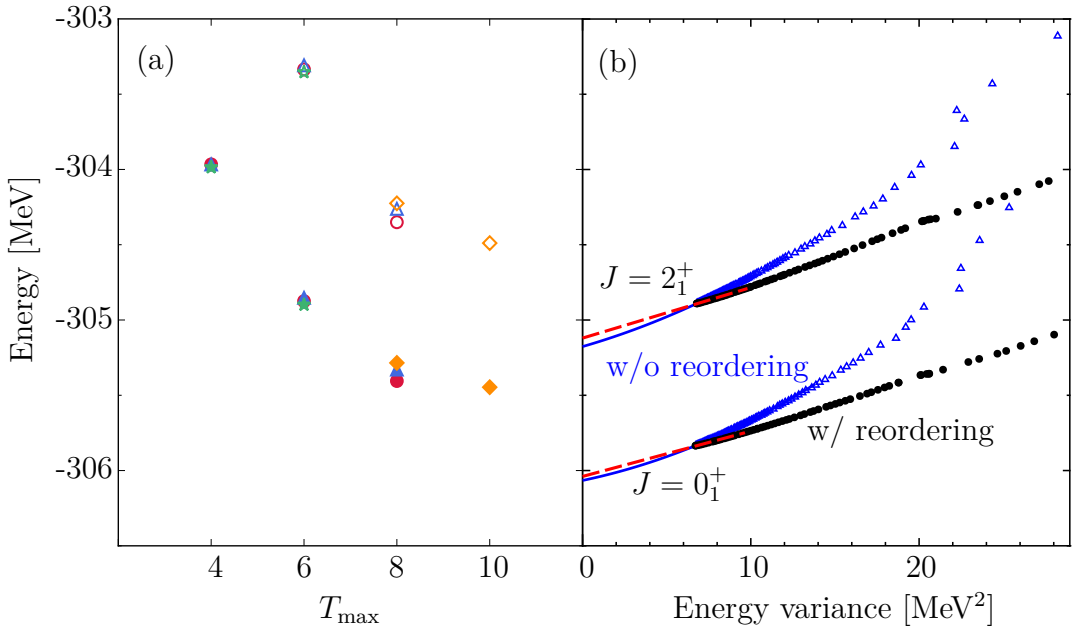

Figure 6.12.: (a) Filled and open symbols denote energies of the ground state and first excited state, respectively. The data points represent the eigenenergies obtained in various IT-SM calculations for ^{64}Ge: The reference thresholds $C_{\min} = 2 \times 10^{-4}$ (●) and $C_{\min} = 5 \times 10^{-4}$ (▲) are used for IT-SM calculations starting from a conventional shell-model calculation with $T_{\max} = 4$. For comparison, the energy eigenvalues are shown using the original nuclear Hamiltonian ($\beta = 0$) for the solution of the eigenvalue problem, using $C_{\min} = 2 \times 10^{-4}$ as reference threshold in the IT-SM calculations (★). Furthermore, IT-SM results are given for $C_{\min} = 3 \times 10^{-4}$ where the model space is constructed for the simultaneous description of only three eigenstates (◆). (b) Energy of the ground state and the first excited state obtained in MCSM calculations versus energy variance, see Figure 5.1.

Finally, we study the effects of different reference thresholds, the number of eigenstates the importance-truncated model space is constructed for and center-of-mass contaminations on the IT-SM eigenvalues. Figure 6.12 (a) shows the energies of the ground state and the first excited state for several IT-SM calculations. Figure 6.12 (b) is identical to Figure 5.1 and is repeated in order to illustrate the deviations of the results obtained in the IT-SM and the MCSM. We first consider the effect of the introduction of the center-of-mass Hamiltonian: The energies computed using the Hamiltonian given in (6.10) are consistently higher for $\beta = 1$ than the energies obtained in an IT-SM calculation using $\beta = 0$. The eigenstates have coupled intrinsic and center-of-mass components and are thus shifted to higher energies for $\beta = 1$. The energies corresponding to smaller reference thresholds are better approximations to the exact values because the respective importance-truncated model spaces are larger and therefore better suited to describing the eigenstates. Note that the energies obtained in an

IT-SM calculation for $C_{\mathrm{min}} = 3 \times 10^{-4}$ are higher than the respective energies computed using the reference threshold $C_{\mathrm{min}} = 5 \times 10^{-4}$ because the importance-truncated model space has been constructed for the simultaneous description of only three eigenstates. An importance-truncated model space including basis states needed for the description of several eigenstates improves the basis expansion of each eigenstate because it contains more basis states than the corresponding importance-truncated model space constructed for the description of a single eigenstate. We conclude from the weak T_{max} dependence of the last two data points that the energies are already approximately converged for $T_{\mathrm{max}} = 10$. However, ^{64}Ge is a deformed nucleus and we would need to go to large T_{max} in order to account for all relevant particle-hole excitations. We will investigate the effect of larger values of T_{max} on the energies. We will also carry out IT-SM calculations for smaller thresholds in order to improve the results. Finally, we remark that the MCSM is a very involved approach [6] whereas the IT-SM is a conceptually simple extension of the conventional shell modell to larger model spaces.

Chapter 7

Conclusion and Outlook

We have applied the importance-truncation scheme to the valence-space shell model in order to extend it to larger model spaces. The conventional shell model successfully describes medium-mass and heavy nuclei in model spaces containing up to 10^{10} basis states. The model-space dimensions increase rapidly when including higher numbers of valence nucleons and single-particle orbits in the valence space. Thus, many nuclei and valence spaces remain out of reach of standard shell-model calculations. In order to overcome these limitations, we introduce an importance measure derived from multi-configurational perturbation theory that estimates the relevance of the individual basis states for the basis expansion of the target eigenstates *a priori*, i.e. without actually solving the eigenvalue problem of the Hamiltonian. Only basis states with an importance measure larger than a given importance threshold are included in the importance-truncated model space. We solve the eigenvalue problem in this dramatically reduced model space and obtain variational approximations to the exact eigenstates, which are recovered in the limit of vanishing thresholds. Based on this property, we use a numerical extrapolation of the IT-SM results in order to account approximately for effects of configurations excluded from the importance-truncated model space.

We perform IT-SM calculations simultaneously for several target eigenstates. Using ^{56}Ni and ^{64}Ge as test cases, we compute energies and electromagnetic observables in the framework of the IT-SM. For ^{56}Ni, we employ the KB3 interaction in the pf shell, and we use the PFG9B3 interaction in the $pfg_{9/2}$ shell for ^{64}Ge. The results demonstrate the efficiency of the importance-truncation scheme: The model-space sizes are reduced significantly while the results are in good agreement with conventional shell-model calculations where the latter are feasible. Note that ^{64}Ge is already beyond the reach of standard shell-model calculations, but has been considered in the framework of the Monte-Carlo shell model. Although we are still working on the corresponding IT-SM

calculations for this complex nucleus, we can already confirm reasonable agreement between the results of both approaches. We conclude that the IT-SM allows to access larger T_{max} spaces and heavier nuclei than the conventional shell model, which is a crucial step for the consistent description of nuclei all over the nuclear chart.

In the future, we will employ the IT-SM to systematically study nuclei beyond the reach of the conventional shell model and investigate the evolution of shell structure. We will predict nuclear properties such as energies and electromagnetic observables for nuclei where no experimental data are available. For these calculations, we will also use new shell-model interactions derived from chiral effective field theory in the framework of the in-medium similarity renormalization group [49, 50] and test their reliability. Furthermore, we will optimize the performance of our IT-SM code and extend it to the computation of a variety of observables, e.g. Gamow-Teller transitions and strength functions.

Appendix A

Multi-Configurational Perturbation Theory

In Section 4.2, we have derived the lowest orders of the energy and state corrections in multi-configurational perturbation theory. This framework implies the splitting of the Hamiltonian into an unperturbed part and a perturbation,

$$\mathbf{H} = \mathbf{H}_0 + \mathbf{W}. \tag{A.1}$$

We have defined the unperturbed Hamiltonian as

$$\mathbf{H}_0 = \epsilon_{\mathrm{ref}} \left|\Psi_{\mathrm{ref}}\right\rangle \left\langle\Psi_{\mathrm{ref}}\right| + \sum_{\nu \notin \mathcal{M}_{\mathrm{ref}}} \epsilon_\nu \left|\Phi_\nu\right\rangle \left\langle\Phi_\nu\right|, \tag{A.2}$$

see Equation (4.7). This Hamiltonian has been chosen in such a way that it fulfills the eigenvalue relation (4.6). Eigenstates of $\mathbf{H}_0$ within $\mathcal{M}_{\mathrm{ref}}$ that are orthogonal to the reference state $\left|\Psi_{\mathrm{ref}}\right\rangle$ do not contribute to the energy and state corrections and have therefore been omitted from the outset in the definition of the unperturbed Hamiltonian.

In the following, we justify this ansatz by defining the "complete" unperturbed Hamiltonian

$$\mathbf{H}_0' = \sum_{\rho \in \mathcal{M}_{\mathrm{ref}}} \epsilon_\rho \left|\Psi_\rho\right\rangle \left\langle\Psi_\rho\right| + \sum_{\nu \notin \mathcal{M}_{\mathrm{ref}}} \epsilon_\nu \left|\Phi_\nu\right\rangle \left\langle\Phi_\nu\right| \tag{A.3}$$

and deriving the lowest orders of the energy and state corrections again. In the definition of $\mathbf{H}_0'$, the relations $\epsilon_\rho = \epsilon_{\mathrm{ref}}$ and $\left|\Psi_\rho\right\rangle = \left|\Psi_{\mathrm{ref}}\right\rangle$ hold for one ρ.

We derive the first-order energy correction starting from Equation (4.15):

$$\langle\Psi_{\text{ref}}|\mathbf{H}_0'|\Psi^{(1)}\rangle + \langle\Psi_{\text{ref}}|\mathbf{W}|\Psi_{\text{ref}}\rangle = \epsilon_{\text{ref}}\langle\Psi_{\text{ref}}|\Psi^{(1)}\rangle + E^{(1)}\langle\Psi_{\text{ref}}|\Psi_{\text{ref}}\rangle\,. \tag{A.4}$$

As in Section 4.2, we apply the eigenvalue relation

$$\mathbf{H}_0'\,|\Psi_{\text{ref}}\rangle = \epsilon_{\text{ref}}\,|\Psi_{\text{ref}}\rangle \tag{A.5}$$

in the first term, yielding

$$\epsilon_{\text{ref}}\langle\Psi_{\text{ref}}|\Psi^{(1)}\rangle + \langle\Psi_{\text{ref}}|\mathbf{W}|\Psi_{\text{ref}}\rangle = \epsilon_{\text{ref}}\langle\Psi_{\text{ref}}|\Psi^{(1)}\rangle + E^{(1)}\langle\Psi_{\text{ref}}|\Psi_{\text{ref}}\rangle\,. \tag{A.6}$$

Thus, the first-order energy correction is given by:

$$E^{(1)} = \langle\Psi_{\text{ref}}|\mathbf{W}|\Psi_{\text{ref}}\rangle = 0. \tag{A.7}$$

This result is identical to that of Section 4.2, where we have used the simple version of the unperturbed Hamiltonian.

The second-order energy correction

$$E^{(2)} = \langle\Psi_{\text{ref}}|\mathbf{W}|\Psi^{(1)}\rangle \tag{A.8}$$

is identical to Equation (4.37) if the first-order state correction is the same as in Section 4.2.

The first-order state correction can be expanded in terms of the basis states of the full model space:

$$|\Psi^{(1)}\rangle = \sum_{\nu\in\mathcal{M}_{\text{full}}} |\Phi_\nu\rangle\langle\Phi_\nu|\Psi^{(1)}\rangle\,. \tag{A.9}$$

We determine the coefficient $\langle\Phi_\nu|\Psi^{(1)}\rangle$ using (A.3) as unperturbed Hamiltonian. Again, we start from Equation (4.23),

$$\langle\Phi_\nu|\mathbf{H}_0'|\Psi^{(1)}\rangle + \langle\Phi_\nu|\mathbf{W}|\Psi_{\text{ref}}\rangle = \epsilon_{\text{ref}}\langle\Phi_\nu|\Psi^{(1)}\rangle\,, \tag{A.10}$$

and consider basis states $|\Phi_\nu\rangle$ belonging to the reference space and outside the reference space separately:

- $|\Phi_\nu\rangle \in \mathcal{M}_{\text{ref}}$:
  We show that $\langle\Phi_\nu|\mathbf{H}_0'|\Psi^{(1)}\rangle$ vanishes in the same way as in Section 4.2:

$$\langle\Phi_\nu|\mathbf{H}_0'|\Psi^{(1)}\rangle = \sum_{\rho\in\mathcal{M}_{\text{ref}}} \epsilon_\rho \langle\Phi_\nu|\Psi_\rho\rangle \langle\Psi_\rho|\Psi^{(1)}\rangle + \sum_{\mu\notin\mathcal{M}_{\text{ref}}} \epsilon_\mu \langle\Phi_\nu|\Phi_\mu\rangle \langle\Phi_\mu|\Psi^{(1)}\rangle . \tag{A.11}$$

  The last term vanishes because the states $|\Phi_\nu\rangle$ and $|\Phi_\mu\rangle$ belong to orthogonal model spaces. In order to show that the remaining right-hand side of Equation (A.11) vanishes, we multiply (4.14) by an arbitrary eigenstate $\langle\Psi_\rho|$ of the unperturbed Hamiltonian:

$$\langle\Psi_\rho|\mathbf{H}_0'|\Psi^{(1)}\rangle + \langle\Psi_\rho|\mathbf{W}|\Psi_{\text{ref}}\rangle = \epsilon_{\text{ref}} \langle\Psi_\rho|\Psi^{(1)}\rangle + E^{(1)} \langle\Psi_\rho|\Psi_{\text{ref}}\rangle . \tag{A.12}$$

  Since the eigenstate $|\Psi_\rho\rangle$ of the unperturbed Hamiltonian is a linear combination of basis states of the reference space, the second term vanishes due to (4.20) and we are left with

$$\langle\Psi_\rho|\mathbf{H}_0'|\Psi^{(1)}\rangle = \epsilon_{\text{ref}} \langle\Psi_\rho|\Psi^{(1)}\rangle . \tag{A.13}$$

  The left-hand side yields

$$\langle\Psi_\rho|\mathbf{H}_0'|\Psi^{(1)}\rangle = \sum_{\sigma\in\mathcal{M}_{\text{ref}}} \epsilon_\sigma \langle\Psi_\rho|\Psi_\sigma\rangle \langle\Psi_\sigma|\Psi^{(1)}\rangle + \sum_{\nu\notin\mathcal{M}_{\text{ref}}} \epsilon_\nu \langle\Psi_\rho|\Phi_\nu\rangle \langle\Phi_\nu|\Psi^{(1)}\rangle \tag{A.14}$$

$$= \epsilon_\rho \langle\Psi_\rho|\Psi^{(1)}\rangle , \tag{A.15}$$

  where we have used the normalization $\langle\Psi_\rho|\Psi_\sigma\rangle = \delta_{\rho,\sigma}$. The second term in (A.14) vanishes because the states $|\Psi_\rho\rangle$ and $|\Phi_\nu\rangle$ belong to orthogonal spaces and do not overlap. Thus, Equation (A.13) reduces to

$$\epsilon_\rho \langle\Psi_\rho|\Psi^{(1)}\rangle = \epsilon_{\text{ref}} \langle\Psi_\rho|\Psi^{(1)}\rangle . \tag{A.16}$$

  This relation only holds for $|\Psi_\rho\rangle = |\Psi_{\text{ref}}\rangle$, for which the coefficient $\langle\Psi_\rho|\Psi^{(1)}\rangle = \langle\Psi_{\text{ref}}|\Psi^{(1)}\rangle$ vanishes anyway due to the intermediate normalization (4.17). For $|\Psi_\rho\rangle \neq |\Psi_{\text{ref}}\rangle$, the scalar product $\langle\Psi_\rho|\Psi^{(1)}\rangle$ is required to vanish in order to fulfill (A.16). Thus, we have

$$\langle\Phi_\nu|\Psi^{(1)}\rangle = 0 \qquad \forall\ |\Phi_\nu\rangle \in \mathcal{M}_{\text{ref}} \tag{A.17}$$

  as in Section 4.2 and basis states of the reference space do not contribute to the

basis expansion of the first-order correction to the eigenstate.

- $|\Phi_\nu\rangle \notin \mathcal{M}_{\text{ref}}$:
  In this case, the first term of Equation (A.10) yields

$$\langle\Phi_\nu|\mathbf{H}_0'|\Psi^{(1)}\rangle = \sum_{\rho\in\mathcal{M}_{\text{ref}}} \epsilon_\rho \langle\Phi_\nu|\Psi_\rho\rangle \langle\Psi_\rho|\Psi^{(1)}\rangle + \sum_{\mu\notin\mathcal{M}_{\text{ref}}} \epsilon_\mu \langle\Phi_\nu|\Phi_\mu\rangle \langle\Phi_\mu|\Psi^{(1)}\rangle \tag{A.18}$$

$$= \sum_{\mu\notin\mathcal{M}_{\text{ref}}} \epsilon_\mu \langle\Phi_\nu|\Phi_\mu\rangle \langle\Phi_\mu|\Psi^{(1)}\rangle \tag{A.19}$$

$$= \epsilon_\nu \langle\Phi_\nu|\Psi^{(1)}\rangle . \tag{A.20}$$

  We therefore obtain the same coefficient,

$$\langle\Phi_\nu|\Psi^{(1)}\rangle = -\frac{\langle\Phi_\nu|\mathbf{W}|\Psi_{\text{ref}}\rangle}{\epsilon_\nu - \epsilon_{\text{ref}}} \qquad \forall\ |\Phi_\nu\rangle \notin \mathcal{M}_{\text{ref}}, \tag{A.21}$$

  as for the simple form of the unperturbed Hamiltonian, see Equation (4.30).

We conclude that we obtain the same state and energy corrections if employing the simplified unperturbed Hamiltonian (A.2) instead of (A.3) and that the use of the former is justified.

Bibliography

[1] M. G. Mayer: *On closed shells in nuclei. ii.* Phys. Rev. 75: 1969, 1949.

[2] O. Haxel, J. H. D. Jensen and H. E. Suess: *On the "magic numbers" in nuclear structure.* Phys. Rev. 75: 1766, 1949.

[3] S. M. Lenzi, F. Nowacki, A. Poves and K. Sieja: *The Land of deformation south of ^{68}Ni.* arXiv 1009.1846, 2010.

[4] E. Caurier and F. Nowacki: *Present status of shell model techniques.* Acta Physica Polonica B 30: 705, 1999.

[5] R. Roth: *Importance truncation for large-scale configuration interaction approaches.* Phys. Rev. C 79: 064324, 2009.

[6] T. Otsuka, M. Honma, T. Mizusaki, N. Shimizu and Y. Utsuno: *Monte carlo shell model for atomic nuclei.* Progress in Particle and Nuclear Physics 47: 319, 2001.

[7] A. Bohr and A. Ben R. Mottelson: *Nuclear Structure: Single-particle motion.* Nuclear Structure. World Scientific, 1969.

[8] L. Coraggio, A. Covello, A. Gargano, N. Itaco and T. Kuo: *Shell-model calculations and realistic effective interactions.* Progress in Particle and Nuclear Physics 62: 135 , 2009.

[9] R. B. Wiringa, R. A. Smith and T. L. Ainsworth: *Nucleon-nucleon potentials with and without $\delta(1232)$ degrees of freedom.* Phys. Rev. C 29: 1207, 1984.

[10] R. Machleidt, K. Holinde and C. Elster: *The bonn meson-exchange model for the nucleon—nucleon interaction.* Physics Reports 149: 1 , 1987.

[11] D. R. Entem and R. Machleidt: *Accurate charge-dependent nucleon-nucleon potential at fourth order of chiral perturbation theory.* Phys. Rev. C 68: 041001, 2003.

[12] E. Epelbaum, W. Glöckle and U.-G. Meissner: *The two-nucleon system at next-to-next-to-next-to-leading order.* Nuclear Physics A 747: 362 , 2005.

[13] B. H. BRANDOW: *Linked-cluster expansions for the nuclear many-body problem.* Rev. Mod. Phys. 39: 771, 1967.

[14] K. A. Brueckner and C. A. Levinson: *Approximate reduction of the many-body problem for strongly interacting particles to a problem of self-consistent fields.* Phys. Rev. 97: 1344, 1955.

[15] B. D. Day: *Elements of the brueckner-goldstone theory of nuclear matter.* Rev. Mod. Phys. 39: 719, 1967.

[16] S. Bonger, T. Kuo and L. Coraggio: *Low momentum nucleon–nucleon potentials with half-on-shell t-matrix equivalence.* Nuclear Physics A 684: 432 , 2001.

[17] S. Bogner, T. T. S. Kuo, L. Coraggio, A. Covello and N. Itaco: *Low momentum nucleon-nucleon potential and shell model effective interactions.* Phys. Rev. C 65: 051301, 2002.

[18] C. Bloch and J. Horowitz: *Sur la détermination des premiers états d'un système de fermions dans le cas dégénéré.* Nuclear Physics 8: 91 , 1958.

[19] T. Kuo, S. Lee and K. Ratcliff: *A folded-diagram expansion of the model-space effective hamiltonian.* Nuclear Physics A 176: 65 , 1971.

[20] K. Suzuki and S. Y. Lee: *Convergent theory for effective interaction in nuclei.* Progress of Theoretical Physics 64: 2091, 1980.

[21] E. Caurier, G. Martinez-Pinedo, F. Nowacki, A. Poves and A. P. Zuker: *The shell model as a unified view of nuclear structure.* Reviews of Modern Physics 77: 427, 2005.

[22] M. Hjorth-Jensen, T. T. Kuo and E. Osnes: *Realistic effective interactions for nuclear systems.* Physics Reports 261: 125 , 1995.

[23] C. Lanczos: *An iteration method for the solution of the eigenvalue problem of linear differential and integral operators.* J. Res. Natl. Bur. Stand. B Math. Sci. 45: 255, 1950.

[24] T. Sebe and J. Nachamkin: *Variational buildup of nuclear shell model bases.* Annals of Physics 51: 100 , 1969.

[25] R. Whitehead: *A numerical approach to nuclear shell-model calculations.* Nuclear Physics A 182: 290 , 1972.

[26] R. B. Lehoucq, D. C. Sorensen and C. Yang: *ARPACK Users' Guide: Solution of Large Scale Eigenvalue Problems with Implicitly Restarted Arnoldi Methods*, 1997.

[27] M. Honma, T. Otsuka, B. Brown and T. Mizusaki: *Shell-model description of neutron-rich pf shell nuclei with a new effective interaction gxpf1.* Eur. Phys. J. A 25: 499, 2005.

[28] M. Horoi, B. A. Brown, T. Otsuka, M. Honma and T. Mizusaki: *Shell model analysis of the* ^{56}Ni *spectrum in the full pf model space.* Phys. Rev. C 73: 061305, 2006.

[29] T. Mizusaki: *Riken accel. prog. rep.* Tech. rep., 2000.

[30] D. Gloeckner and R. Lawson: *Spurious center-of-mass motion.* Physics Letters B 53: 313 , 1974.

[31] D. J. Dean, M. T. Ressell, M. Hjorth-Jensen, S. E. Koonin, K. Langanke and A. P. Zuker: *Shell-model monte carlo studies of neutron-rich nuclei in the* $1s - 0d - 1p - 0f$ *shells.* Phys. Rev. C 59: 2474, 1999.

[32] R. Whitehead, A. Watt, B. Cole and I. Morrison: *Computational Methods for Shell Model Calculations.* Adv. Nucl. Phys. 9: 123, 1977.

[33] P. Surján, Z. Rolik, Á. Szabados and D. Kőhalmi: *Partitioning in multiconfiguration perturbation theory.* Ann. Phys. 13: 223, 2004.

[34] E. Hylleraas and B. Undheim: Z. Phys. 65: 759, 1930.

[35] A. Poves and A. Zuker: *Theoretical spectroscopy and the fp shell.* Physics Reports 70: 235 , 1981.

[36] E. Caurier: *Shell model code ANTOINE.* IRES, STRASBOURG, 1989-2004.

[37] R. Buenker and S. Peyerimhoff: *Energy extrapolation in ci calculations.* Theoretica chimica acta 39: 217, 1975.

[38] M. Honma, T. Mizusaki and T. Otsuka: *Diagonalization of hamiltonians for many-body systems by auxiliary field quantum monte carlo technique.* Phys. Rev. Lett. 75: 1284, 1995.

[39] J. Hubbard: *Calculation of partition functions.* Phys. Rev. Lett. 3: 77, 1959.

[40] R. L. Stratonovich: *On a Method of Calculating Quantum Distribution Functions.* Soviet Physics Doklady 2: 416, 1957.

[41] J. Egido, J. Lessing, V. Martin and L. Robledo: *On the solution of the hartree-fock-bogoliubov equations by the conjugate gradient method.* Nuclear Physics A 594: 70 , 1995.

[42] N. Shimizu, Y. Utsuno, T. Mizusaki, M. Honma, Y. Tsunoda and T. Otsuka: *Variational procedure for nuclear shell-model calculations and energy-variance extrapolation.* Phys. Rev. C 85: 054301, 2012.

[43] M. Honma and et. al.: unpublished.

[44] T. Otsuka: private communication.

[45] H. Junde, H. Su and Y. Dong: *Nuclear data sheets for $a = 56$.* Nuclear Data Sheets 112: 1513 , 2011.

[46] M. Honma, T. Otsuka, B. A. Brown and T. Mizusaki: *New effective interaction for pf-shell nuclei and its implications for the stability of the $n = z = 28$ closed core.* Phys. Rev. C 69: 034335, 2004.

[47] J. Suhonen: *From Nucleons to Nucleus.* Theoretical and Mathematical Physics. Springer London, Limited, 2007. ISBN 9783540488613.

[48] B. Singh: *Nuclear data sheets for $a = 64$.* Nuclear Data Sheets 108: 197 , 2007.

[49] H. Hergert, S. K. Bogner, S. Binder, A. Calci, J. Langhammer, R. Roth and A. Schwenk: *In-medium similarity renormalization group with chiral two- plus three-nucleon interactions.* Phys. Rev. C 87: 034307, 2013.

[50] K. Tsukiyama, S. K. Bogner and A. Schwenk: *In-medium similarity renormalization group for open-shell nuclei.* Phys. Rev. C 85: 061304, 2012.

Danksagung

Es gibt sehr viele Menschen, die mich vor und während dieser Arbeit unterstützt und damit erheblich zu deren Gelingen beigetragen haben.

Nun möchte ich die Gelegenheit nutzen, einmal Danke zu sagen.

Ich möchte mich ganz herzlich bei Herr Prof. Roth für die Möglichkeit bedanken, dieses spannende Thema zu bearbeiten und diese Arbeit anzufertigen. Vielen Dank für die freundliche Aufnahme in Ihre Arbeitsgruppe und die hervorragende Betreuung während des ganzen letzten Jahres.

Außerdem möchte ich mich bei der gesamten Arbeitsgruppe für die angenehme Atmosphäre und die Hilfsbereitschaft bei physikalischen oder technischen Problemen bedanken. Insbesondere möchte ich mich bei Eskendr Gebrerufael, Alexander Tichai, Richard Trippel und Roland Wirth für die tolle Bürogemeinschaft, die vielen interessanten Diskussionen und die Hilfe bei Problemen jeglicher Art bedanken. In diesem Zusammenhang möchte ich besonders Roland danken für die Hilfe bei Computerproblemen und das Korrekturlesen dieser Arbeit.

Ganz besonderer Dank geht natürlich an meine ganze Familie, allen voran an meine Eltern, Angelika und Klaus Stumpf, und meine Schwester Steffi. Danke, dass ihr mir es finanziell ermöglicht habt, zu studieren und dass ihr mich immer wieder motiviert und mir zur Seite steht.

Herzlicher Dank geht an meinen Freund Benjamin Bastida Virgili. Danke für deine Liebe, dein Verständnis und deine Unterstützung während meines Studiums. Danke, dass du für mich da bist und es schaffst, mich zu entspannen und mich zum Lachen zu bringen, wann immer ich es nötig habe. Damit warst du mir insbesondere in der Schlussphase meiner Masterarbeit die größte Stütze von allen. Moltes gràcies!

Erklärung zur Eigenständigkeit

Hiermit versichere ich, die vorliegende Master-Thesis ohne Hilfe Dritter nur mit den angegebenen Quellen und Hilfsmitteln angefertigt zu haben. Alle Stellen, die aus diesen Quellen entnommen wurden, sind als solche kenntlich gemacht worden. Diese Arbeit hat in gleicher oder ähnlicher Form noch keiner Prüfungsbehörde vorgelegen.

Ort und Datum

Christina Stumpf